Seasonal variability in silicate weathering signatures recorded by Li isotopes in cave drip-waters

David J. Wilson[a,*], Philip A.E. Pogge von Strandmann[a,b], Jo White[a], Gary Tarbuck[a], Alina D. Marca[c], Tim C. Atkinson[a], Philip J. Hopley[a]

[a]*London Geochemistry and Isotope Centre (LOGIC), Institute of Earth and Planetary Sciences, University College London and Birkbeck, University of London, Gower Street, London, WC1E 6BT, U.K.*

[b]*Institute of Geosciences, Johannes Gutenberg University, 55122 Mainz, Germany.*

[c]*School of Environmental Sciences, University of East Anglia, Norwich, NR4 7TJ, U.K.*

* Corresponding Author. Tel.: +44 20 3108 6349. Email: david.j.wilson@ucl.ac.uk

Contents:
abstract (333 words)
highlights
key words
main text (11027 words)
references (93)
figures (9)
tables (2)

Electronic Annex (5 supp tables, 2 supp figures)

Revised version for *Geochimica et Cosmochimica Acta*

5th June 2021

Highlights

- Time series of soil porewater chemistry from drip-waters in Yorkshire caves
- Drip-water lithium isotopes vary spatially and temporally from δ^7Li = +1 ‰ to +17 ‰
- Temporal variability arises from lithium incorporation into secondary phases
- Possible controls by seasonal changes in temperature and/or fluid residence time
- Seasonal variability should be considered when interpreting paleo-proxy records

Key words

chemical weathering; carbon cycle; climate; seasonality; geochemistry; lithium isotopes; porewater; caves

Abstract

Silicate weathering is a critical process in Earth's carbon cycle, but the fundamental controls on weathering are poorly understood and its response to future climate change is uncertain. In particular, the potential for changes in seasonality or extreme weather events to control silicate weathering rates or mechanisms has been little studied. Here, we use lithium (Li) isotope measurements in bimonthly sampled drip-waters from two caves in the Yorkshire Dales (U.K.) to assess the response of silicate weathering processes to changes in temperature and hydrology over seasonal timescales. While the caves are contained in limestone bedrock, the drip-water Li isotope signal predominantly reflects silicate weathering of the overlying soils that are dominated by glacial till.

Drip-water Li isotope compositions record spatial and temporal variability ranging from δ^7Li values of +1 to +17 ‰, with a mean of +11 ‰. These values are significantly higher than local lithogenic inputs (δ^7Li = -1 ± 1 ‰), consistent with isotope fractionation during secondary mineral formation. Comparison to temperature, precipitation, drip rates, and drip-water chemistry enables the controls on the Li isotope weathering signatures to be explored, revealing possible roles for both temperature and fluid residence time in setting the balance between primary rock dissolution and secondary mineral formation. Specifically, our Li isotope data are consistent with a scenario in which cooler temperatures and/or longer fluid residence times lead to enhanced secondary mineral formation relative to silicate dissolution.

Overall, our results indicate the potential for Li isotope variability over short temporal and spatial scales, which is important to consider when interpreting past changes in weathering processes or fluxes from paleo-records. In addition, the seasonal changes in Li isotopes suggest that weathering processes may be sensitive to seasonality or to extreme weather events, rather than responding only to the mean climate state. With warmer temperatures and more intense rainfall events expected in future, both increased primary rock dissolution and enhanced weathering efficiency (due to reduced secondary mineral formation) could potentially contribute to increased carbon dioxide drawdown by silicate weathering.

1. Introduction

Chemical weathering of silicate rocks is a key process that controls Earth's geochemical and carbon cycles, and hence global climate (Walker et al., 1981; Berner et al., 1983), but the strength of the climate-weathering feedback and the timescales it operates over are poorly constrained (e.g. West, 2012; Li et al., 2016; Krissansen-Totton and Catling, 2017). Given the significant uncertainty in how, and how fast, weathering will respond to future climate change, it is essential to obtain a better understanding of the controls on weathering. Lithium (Li) isotopes are a promising tracer for this purpose because they are uniquely sensitive to silicate weathering processes (Dellinger et al., 2015; Pogge von Strandmann et al., 2017a) and insensitive to both carbonate weathering (Kısakűrek et al., 2005) and biological effects (Lemarchand et al., 2010; Clergue et al., 2015; Pogge von Strandmann et al., 2016). Lithium isotope records from marine carbonates have been used to constrain globally-integrated changes in weathering fluxes and/or processes in response to climate over multi-kyr to Myr timescales (Hathorne and James, 2006; Misra and Froelich, 2012; Pogge von Strandmann et al., 2017b). In addition, speleothems can record localised changes in weathering processes over tens to thousands of years (Pogge von Strandmann et al., 2017c), while authigenic clay minerals may be another promising archive of paleo-fluid compositions in weathering systems (Clauer et al., 2018). However, chemical weathering could also vary over much shorter timescales (Gislason et al., 2009), in which case both paleo-records and the future global carbon cycle may be sensitive to changes in seasonality or to extreme weather events, rather than responding only to the mean climate state.

Lithium isotopes trace weathering processes because rock dissolution is approximately congruent for Li isotopes whereas the formation of secondary minerals such as clays and oxides preferentially removes ^{6}Li and leaves the weathering solution enriched in ^{7}Li (Pistiner and Henderson, 2003; Vigier et al., 2008; Wimpenny et al., 2010; Dellinger et al., 2015; Pogge von Strandmann et al., 2017a; Hindshaw et al., 2019a). Hence, Li isotopes in soil porewaters or river waters should trace the balance between silicate rock dissolution and secondary mineral formation. Importantly, the formation of secondary clays sequesters some of the cations released during rock dissolution, which can reduce the efficiency of carbon dioxide drawdown during weathering (Pogge von Strandmann and Henderson, 2015). Therefore, Li isotopes potentially provide a tool for quantifying changes in both silicate weathering processes and the efficiency of carbon sequestration by weathering.

Measurements of Li isotopes in river waters reflect modern weathering processes at a catchment scale, but 'snapshot' sampling at single points in time has only recently been extended to time series sampling, allowing seasonal changes to be revealed (Liu et al., 2015; Gou et al., 2019; Hindshaw et al., 2019b). In some settings, seasonal variability in Li isotopes could reflect temperature-dependent isotopic fractionation (Gou et al., 2019), but in other cases

it hints at a role for fluid residence time in controlling weathering processes (Liu et al., 2015; Hindshaw et al., 2019b). In addition, seasonal variations in river water chemistry may also be influenced by mixing between different fluid reservoirs, such as soil porewaters and deep groundwaters (Tipper et al., 2006; Calmels et al., 2011; Fries et al., 2019; Hindshaw et al., 2019b), rather than necessarily recording fundamental changes in weathering processes. Given also that a large proportion of weathering occurs in soils rather than in rivers, complementary constraints on temporal variability in soil weathering processes are required. However, obtaining soil porewater time series is challenging, so most Li isotope studies on porewaters have only involved snapshot sampling (e.g. Pogge von Strandmann et al., 2012; Steinhoefel et al., 2021) or limited repeat measurements (e.g. Lemarchand et al., 2010; Fries et al., 2019), rather than continuous time series.

Here we develop an approach to obtain time series of soil porewater Li isotope compositions using cave drip-waters collected over a two-year period in Pippikin and White Scar caves in the Yorkshire Dales, U.K. The former cave is technically challenging to access, whereas the latter is a show cave that is open to the public. Since the drip-waters are sourced from the overlying soil porewaters before flowing through limestone, these samples contain a record of the temporally evolving weathering fluid chemistry. In theory, silicate weathering and secondary mineral formation in the soils will control the Li isotope compositions of the weathering fluids, with little or no effect from the underlying carbonates (Kısakűrek et al., 2005; Millot et al., 2010b; Pogge von Strandmann et al., 2017a). Therefore, these Li isotope time series enable a first-order quantification of seasonal variability in silicate weathering processes and signatures. In combination with records of temperature, precipitation, drip rates, and drip-water chemistry, we explore the controls on weathering, and specifically assess the possible roles of temperature and fluid residence time in setting the balance between rock dissolution and secondary clay formation. An improved understanding of how chemical weathering processes in soils are recorded by Li isotopes is important for interpreting both modern river data and paleo-records of Li isotope changes, which will feed into a better understanding of how changes in temperature, seasonality, and hydrological processes will impact on the future global carbon cycle.

2. Regional setting and samples

Drip-water samples were collected from two caves in the Yorkshire Dales, U.K.: Pippikin Pot via its Mistral entrance in the Ease Gill Cavern system (Grid Reference SD 667 803), and White Scar Cave beneath Ingleborough (Grid Reference SD 712 745). Descriptions of the caves and their geological setting are given in Waltham and Lowe (2017). They are ~7 km apart and both are contained within the Great Scar Limestone of Lower Carboniferous age, which comprises sub-horizontally bedded carbonate with occasional cm- to m-scale shale layers (Waltham, 1970; Waters and Lowe, 2017). Regionally, the limestone is overlain by the

Yoredale Group, a cyclic succession of shales, sandstones, and thin limestones, but erosion has completely removed these rocks from the limestone benches overlying the caves (Aitkenhead et al., 2002). Their importance for the present study is that they form the source material for the glacial tills that presently overlie the caves (Mitchell, 1991; Mitchell, 1994; Livingstone et al., 2012). The tills themselves are diamictons, containing predominantly sandstone and limestone clasts in varying proportions, within a poorly-sorted matrix of sand, silt, and clay (Rose, 1991; Murphy et al., 2001). The carbonate content of the matrix is reported to match the proportion of limestone outcropping in the source area (Andrews and King, 1968). An important contrast between the two cave sites is that Pippikin cave is overlain by tills up to 6 m thick on which peaty gleyed podsolic soils have developed, whereas the study sites at White Scar Cave lie beneath the side slope of the Chapel-le-Dale valley, on which limestone outcrops protrude through well-drained brown earth soils formed on till patches less than 1 m in thickness.

Dye tracing studies at White Scar Cave indicate a timescale of days for the initial breakthrough of tracers from injection points in fractures below the soil cover to drip sites in the cave (Bottrell and Atkinson, 1992). Despite this rapid initial transit, most of the tracer is retained for much longer, with mean residence times of 1 to 2 months (Bottrell and Atkinson, 1992). These results indicate that seasonal changes in the trace element chemistry of soil waters (i.e. inputs to the limestone system) can be recorded by sampling cave drip-waters (i.e. outputs). However, the dye tracing also demonstrated that a very small fraction of the tracer was retained in the system for much longer times, and up to six years in one case (Bottrell and Atkinson, 1992).

The drip-water samples analysed here were collected approximately every two months from August 2016 to November 2018, from two different locations in each cave (see Figs. EA1-2 for maps). Pippikin cave samples A and D (hereafter, Pippikin A and D) were collected from a curtain drip ~200 m from the cave entrance and a ceiling drip ~300 m from the cave entrance. White Scar Cave samples 1 and 3 (White Scar 1 and 3) were collected from a stalactite drip ~400 m from the cave entrance and a collection of drips from a flowstone ~420 m from the cave entrance. At both caves, mean annual surface temperatures are ~8 °C and mean monthly temperatures vary seasonally by ~10 °C, whereas seasonal variations are only ~5 °C inside the cave entrance and < 0.5 °C in the cave interior. Mean annual precipitation totals in the Yorkshire Dales are ~1500 mm (Malham Tarn; Burt and Horton, 2003).

Rock and soil samples were also collected from the vicinity of the two caves. Samples from Pippikin cave include: Great Scar Limestone from the cave entrance; an interbedded shale from the nearby Arson Shaft of Ease Gill; Quaternary till from Ease Gill; peaty soil from high ground overlying the cave; and a modern calcareous sediment sample from the floor of the cave. Samples from White Scar Cave include: Great Scar Limestone from near the cave entrance; Yoredale Shale from the overlying hillslopes; and Quaternary till from near the cave entrance.

3. Methods

3.1 Sample preparation

Drip-water samples were collected in pre-cleaned glass bottles and stored in a fridge. They were filtered in the laboratory at 0.2 μm using a cellulose-acetate filter and syringe to ensure complete removal of fine particles (although visible particle content was minimal) and the filtrate was analysed for Li isotopes and major/trace elements. Unfiltered samples were analysed for oxygen isotopes.

All rock and soil samples were dried and crushed with an agate pestle and mortar. In order to aid digestion of the peaty soil and tills, organic carbon was first oxidised using aqua regia. All samples were then subjected to bulk digestion using concentrated HF, HNO_3, and $HClO_4$ in Teflon beakers on a hotplate at 130 °C, followed by steps in concentrated HNO_3 and 6 M HCl. For the Great Scar Limestone samples, leaching was also conducted to separate the carbonate and detrital fractions. The carbonate fraction was extracted by leaching ~100 mg sample in 8 ml 0.1 M HCl for 1 hour (Pogge von Strandmann et al., 2013), enabling an estimated ~40 mg of calcium carbonate to be dissolved. After repeating this leaching step a second time to remove further carbonate, the detrital residue was digested as for the bulk samples, although it should be noted that some minor carbonate likely remained within this operationally-defined residue, so it probably represents a mixed carbonate and silicate signal. In addition, for a subset of the rock and soil samples from Pippikin cave, a Na-acetate leach was used to target the exchangeable fraction, following the method of Tessier et al. (1979) that was recently also applied for measuring Li isotopes (Pogge von Strandmann et al., 2019). Specifically, ~200 mg of sediment was leached in 2 mL 1M Na-acetate, at room temperature and with frequent ultrasonication, followed by centrifugation and collection of the supernatant fluid.

3.2 Lithium isotopes

Lithium separation followed a standard method of elution in 0.2 M HCl through AG50W X-12 resin, with two column passes through different-sized columns to ensure matrix removal (Pogge von Strandmann et al., 2013). Isotopic measurements were performed on a Nu Plasma 3 MC-ICP-MS at UCL, using a Cetac Aridus 2 desolvation system, 'super-lithium' cones, and standard-sample bracketing with the IRMM-016 Li standard (Pogge von Strandmann et al., 2019). Samples were measured at least three times within an analytical session, with each measurement integrating ~50 seconds, and the reported values are the mean and standard deviation (2sd) of these values, given in permil after re-normalising to the NIST-8454 LSVEC standard (Table 1). Accuracy and external reproducibility were assessed using

seawater and USGS standard BCR-2 (Table EA1a,c), which gave δ^7Li values of +31.3 ± 0.6 ‰ (2sd, n=28) and +2.5 ± 0.3 ‰ (n=5), respectively, in good agreement with literature data (James and Palmer, 2000; Jeffcoate et al., 2004; Pogge von Strandmann et al., 2011; Liu et al., 2013; Dellinger et al., 2015; Pogge von Strandmann et al., 2019).

Because Li isotopes are fractionated during ion chromatography, splits were collected before and after the Li collection interval to assess column yields. Although yields above 99, 99.5, or 99.9 % have variously been proposed to indicate good data quality in past studies, it was recently suggested that yields above ~99.8 % are typically required to ensure no resolvable offset between measured and true Li isotope values, at the precision of the current generation of mass spectrometers (Gou et al., 2020). Here, typical yields after two column passes were 99.8-100 %. However, for a few samples, yields were in the range of 99.0-99.7 %, in which case a small but resolvable offset in Li isotopes could arise. For the column procedures in our laboratory, we have estimated that a 1 % loss in yield could lead to an offset of 1.7 ‰ for δ^7Li, based on analyses of seawater samples with differing column yields (Table EA1b). Because we were often sample-limited and not always able to reanalyse samples, for sample measurements where column yields were in the range of 99.0-99.7 %, we retained the Li isotope data but have taken this additional uncertainty into account. Without knowing whether Li was lost from the light or heavy tail, we could not employ a 'correction' to our data. Instead, we estimated the maximum possible δ^7Li offset based on an empirical linear scaling of 1.7 ‰ per 1 % Li loss, and used this value in place of our analytical 2sd uncertainty where it was larger. Such samples are indicated in the version of Table 1 in the Electronic Annex. The typical procedural blank was 0.01-0.04 ng, which was significantly smaller than sample Li amounts (typically 5-10 ng) and did not warrant blank correction.

3.3 Major and trace elements

Major and trace element concentrations were analysed using a Varian 720 ICP-OES and a Varian 820 ICP-MS. Calibration was based on multi-point calibrations with multi-element solutions. Repeat standard analyses allowed drift to be monitored during analytical runs but no drift correction was applied. Accuracy and precision were assessed by analysis of the international reference standards SLRS-4 (Yeghicheyan et al., 2001; Heimburger et al., 2013), NW-TMDA, and BCR-2 (Jochum et al., 2016).

For water analyses (Table 1, Table EA2), the major and minor elements were analysed by ICP-OES (Ca, Mg, Na, K, Si, Sr), with accuracy within ±10 %. Minor and trace elements in the waters were analysed by ICP-MS (Li, B, Al, Ti, Mo, Ba, U), with accuracy within ±4 %, except for B (±14 %) and U (±7 %). For rock digests and leaches (Table 2, Table EA3), major and selected minor/trace elements were analysed by ICP-OES (Al, Fe, Ti, Mg, Ca, Na, K, P, Mn, Ba, Sr, Rb, Li), with accuracy within ±10 % for all elements (Table EA3).

3.4 Oxygen isotopes

Oxygen isotope compositions of the drip-waters were analysed in the Stable Isotope Laboratory at the University of East Anglia. Subsamples of the water were placed in 1.5 mL vials with septa closures and loaded into the auto-sampler tray of a CDRS instrument (Picarro V 1102-i model). Samples were measured in batches, and each sample was injected and measured 6 times using 2.5 µL of water each time. Together with the samples, two secondary international standards (USGS 64444, USGS 67400) and one internal laboratory standard (NTW – Norwich tap water) were measured, each injected 10 times in order to minimise memory effects. Isotopic compositions were calculated using the calibration line based on the secondary international standards and reported in permil with respect to V-SMOW on the V-SMOW – SLAP scale. The precision of the measurements was 0.1 ‰ for $\delta^{18}O$ (1sd) (Table 1).

3.5 Climate and drip rate monitoring

A temperature logger was installed outside the entrance to Pippikin cave to record surface temperatures at 15-minute intervals, from which we calculated monthly average temperatures from September 2016 to December 2018 (Table EA4). Outside of that period, we use temperature data from a nearby weather station in Bingley (Bingley No 2, https://en.tutiempo.net/climate/united-kingdom.html), adjusted for the mean difference of 1 °C between these locations. Monthly rainfall totals were measured by a rain gauge located in Ingleton, ~2 km from White Scar Cave and ~8 km from Pippikin cave, from September 2016 to November 2018 (Table EA4). Outside of that period, we use precipitation data from the weather station Bingley No 2, adjusted by a factor of 1.4 to account for the higher precipitation totals in the study area. Those monthly rain water samples were also collected and stored for analysis of major/trace elements and Li isotopes (Table EA2). A “Stalagmate” drip logger was installed in Pippikin cave, in the same chamber as the Pippikin D drip-water sampling, to measure drip rates at 15-minute intervals, from which we calculated daily averages and monthly-smoothed data (Table EA5). Instantaneous drip rates were also estimated by manual counting at the individual drip-sites on most occasions that samples were collected (Table 1).

4. Results

4.1 Major and trace elements in drip-waters

For the complete drip-water dataset, the average major element concentrations are: Ca (1200 µmol/L), Na (250 µmol/L), Si (69 µmol/L), Mg (43 µmol/L), K (13 µmol/L) (Table 1). The major element chemistry on a Mg-Ca-(Na+K) plot is similar at all sites, being dominated

by Ca (mean for each site in the range of 74-84 %), with some Na (13-23 %), and minor Mg (3 %) and K (1 %) (Fig. 1a). These data indicate the dominance of carbonate weathering sources but also require a silicate component, and potentially also some contribution of Na from rain water. On a plot of Mg/Na versus Ca/Na (Fig. 1b), it becomes clear that congruent dissolution followed by mixing between carbonate and silicate sources (or rain water) cannot provide a simple explanation for the data. Instead, these data additionally appear to require either a significant effect from incongruent dissolution, or preferential Mg removal (with or without Ca removal). Such Mg (and Ca) removal could arise through secondary mineral formation, such as clay or calcite precipitation, with the latter clearly evidenced by the formation of stalactites, stalagmites, and flowstones in the caves.

For the minor and trace elements, average concentrations are: Sr (900 nmol/L), B (600 nmol/L), Al (400 nmol/L), Li (100 nmol/L), Ba (100 nmol/L), Ti (6 nmol/L), Mo (4 nmol/L), U (2 nmol/L) (Table 1). Notably, Li concentrations vary between the sites, being an order of magnitude higher at Pippikin D (mean 450 nmol/L) than at Pippikin A and the White Scar Cave sites (~30 nmol/L). Pippikin D also displays higher Ti, Mo, Ba, and U concentrations, by a factor of around 2 to 3 compared to the other sites, and higher concentrations of certain major elements (Na, K, Mg, and Si are elevated by ~70 %, ~120 %, ~30 %, and ~110 % respectively). Overall, the drip-water Li concentrations are similar to concentrations measured in soil solutions on Guadeloupe (30-100 nmol/L) (Fries et al., 2019), in soil solutions and small streams at the Shale Hills Critical Zone Observatory in the Appalachians (30-120 nmol/L) (Steinhoefel et al., 2021), and in spring waters in the Massif Central (10-300 nmol/L) (Négrel et al., 2010). In contrast, they are mostly at the lower end of concentrations measured in major global rivers (~50-800 nmol/L; mean ~200 nmol/L) (Huh et al., 1998).

In Figure 2, we plot Mg, Sr, B, and Li concentrations through time, normalised to Na to correct for dilution/concentration effects from rain water inputs or evaporation. At all sites, Mg, Sr, and B co-vary to some extent (Fig. 2a-c), indicating a seasonal signal in the drip-water chemistry. In detail, those temporal patterns indicate generally higher values in summer than in winter, with a lag of around 2 months behind temperature changes (Fig. 2a-c). Such a seasonal pattern is not seen for Li concentrations or Li/Na ratios (Fig. 2d). Instead, Li generally covaries with Na, K, and Si (Fig. 3), although the exact relationship differs between locations, with Li/Na, Li/K, and Li/Si ratios up to an order of magnitude higher at Pippikin D than at the other sites. At Pippikin D, the elevated Li concentrations also correlate with Mg, Ti, Mo, and U concentrations through time (Table 1), whereas a link between Li and these trace elements is not observed at the other sites.

4.2 Lithium isotopes in drip-waters

There is both spatial and temporal variability in drip-water Li isotope compositions, with a total range in δ^7Li values from +1 ‰ to +17 ‰ (Fig. 4). Average δ^7Li values were +11.2

± 4.2 ‰ (2sd) for Pippikin A, +9.0 ± 2.3 ‰ for Pippikin D, +10.3 ± 7.8 ‰ for White Scar 1, and +14.4 ± 6.2 ‰ for White Scar 3. As such, typical intra-site variability within each cave was approximately twice as large in White Scar Cave than in Pippikin cave, while mean values in White Scar Cave were ~2 ‰ higher than in Pippikin cave (Fig. 4).

Temporal variations at an individual site were larger than the spatial variations, with a range in δ^7Li values of ~7 ‰ at Pippikin A, ~5 ‰ at Pippikin D, ~13 ‰ at White Scar 1 (~8 ‰ excluding one low value in December 2017), and ~8 ‰ at White Scar 3 (Fig. 4). These variations were often, but not always, coherent through time between sites in the same cave and between the two caves. In particular, all sites recorded a low δ^7Li value of +7-9 ‰ during November 2016, followed by an increase of 4-6 ‰ between January and March 2017 (or between March and June 2017 for Pippikin D) (Fig. 4). The Pippikin cave sites then recorded a gradual decrease from summer 2017 through to winter 2017, reaching low δ^7Li values during early 2018, before increasing again by summer 2018 (latter increase only recorded at Pippikin A due to low drip rates and a lack of samples from Pippikin D) (Fig. 4a). For White Scar Cave, after reaching high values in March 2017, δ^7Li values generally remained elevated, with the exception of a very low value of +1 ‰ at White Scar 1 during December 2017, and a return to low values in November 2018 (only recorded at White Scar 3 due to sample unavailability at White Scar 1) (Fig. 4b). Although the pattern is not entirely consistent from year to year, the full dataset records lower δ^7Li values during autumn and winter (September-February mean ~+9.3 ‰), with lows particularly in November and December, and higher values during spring and summer (March-August mean ~+12.3 ‰).

Drip-waters at Pippikin D generally recorded the lowest Li isotope values (Fig. 4), accompanied by an order of magnitude higher Li concentrations and Li/Na ratios than the other sites (Table 1). The other sites displayed a larger range in Li isotope compositions (Fig. 4), overlapping with Pippikin D but extending to higher values, and a relatively small range in Li/Na ratios (Table 1). At individual sites, there is no clear correlation between Li isotopes and Li/Na ratios, while the links between Li concentrations and other major/trace elements (e.g. Fig. 3) are generally not observed between Li isotopes and major/trace elements.

4.3 Lithium isotopes and concentrations in rocks, soils, and rain waters

Local rocks, sediments, and soils are characterised by a small range in Li isotopes (Table 2; Fig. 5) and have significantly lower δ^7Li values than the cave drip-waters (Fig. 4). The limestone, shale, till, and cave sediments all have δ^7Li values in the range of -2 to 0 ‰ (Fig. 5a), with good agreement between equivalent samples from the two caves, while the peaty soil from Pippikin cave has a δ^7Li value of +2 ‰. At Pippikin cave, the bulk limestone has a low Li content (~0.3 μg/g) that is similar to the Li content of its carbonate fraction (derived from weak HCl leaching), whereas the till, peaty soil, and cave sediment contain ~300 times

more Li and the shale contains ~8000 times more Li (Fig. 5b). At White Scar Cave, the bulk limestone has a slightly higher Li content (~0.9 μg/g) than at Pippikin cave, but its elevated Li content appears to reflect a small silicate component (as revealed by the operationally-defined detrital residue following weak HCl leaching) rather than elevated Li within the carbonate fraction (Fig. 5b). Therefore, the local shale and till at White Scar Cave contain ~200-300 times more Li than the carbonate fraction of the limestone. For both caves, the carbonate fraction of the limestone (derived from weak HCl leaching) has a Li content of ~0.1-0.2 μg/g and an Al/Ca molar ratio of 0.24 mmol/mol, consistent with derivation of the Li isotope signal in that leach from only the carbonate fraction (Pogge von Strandmann et al., 2013; Dellinger et al., 2020). For the shale, till, soil, and cave sediment from the vicinity of Pippikin cave, the exchangeable fraction was extracted using a Na-acetate leach, but is shown to contain a very low Li content, which represents 0.1 % or less of the respective bulk samples (Table 2). Isotopic measurements on those exchangeable fractions gave δ^7Li values of ~+5 ‰ for the till and ~+17 ‰ for the soil (Table 2), which are in a similar range to the porewater compositions inferred from the drip-waters (Fig. 4).

Measurements of trace elements and Li isotopes on local rain water are also reported (Table EA2), with δ^7Li values ranging from 9.2 to 13.9 ‰ between September 2016 and September 2017. However, their mean Li/Na molar ratio of 0.00027 is elevated over values for seawater (from which rain waters in the U.K. are originally derived) by a factor of 5. We therefore suspect that those Li data are affected by contamination, which could arise from dust or anthropogenic sources to rain water (Millot et al., 2010a), and/or from dust or anthropogenic contamination during collection in the rain gauge. The major element data for rain water are consistent with contributions from carbonate and/or silicate dust dissolution (Fig. 1), while anthropogenic contamination is also evident in analyses of contamination-prone elements such as Zn (not shown). We include the rain water data for completeness but, since we cannot rule out dust dissolution or anthropogenic contamination in the rain gauge, we are cautious of interpreting these Li concentration and isotope data as representative of the inputs to the studied cave systems.

5. Discussion

5.1 Origin of drip-water Li isotope variations

The cave drip-waters record δ^7Li values from +1 to +17 ‰ (Table 1, Fig. 4), which could reflect mixing between sources with different Li isotope compositions and/or modification of source compositions due to isotopic fractionation during Li removal processes. Here we address the sources of Li to the drip-waters and the need for Li removal to explain the Li isotope compositions.

5.1.1 Rain water contributions

Rain water is usually an insignificant source of Li to soil solutions, ground waters, and river water (e.g. Huh et al., 2001; Lemarchand et al., 2010; Dellinger et al., 2015; Henchiri et al., 2016; Gou et al., 2019; Golla et al., 2021). Nevertheless, we consider its possible influence on the cave drip-waters because the drip-waters have Li concentrations that are at the low end of typical riverine Li concentrations (Huh et al., 1998). Rain water in the U.K. is mostly derived from seawater and, since both cave sites are located within ~25 km of the coast, the local rain water can be expected to have a similar Li isotope composition to seawater (e.g. Millot et al., 2010a). We therefore use a seawater endmember (i.e. δ^7Li ~+31 ‰, Li/Na molar ratio = 0.000055) to assess rain water contributions. This approach specifically accounts only for marine aerosol sources, while excluding potential Li inputs linked to atmospheric dust dissolution (Lemarchand et al., 2010; Millot et al., 2010a; Négrel et al., 2020). Silicate and carbonate minerals contained in fine-grained dust probably partly dissolve in rain water, which could explain both the major element chemistry of the measured rain water samples (Fig. 1) and offsets in their δ^7Li values from seawater (Table EA2). However, dust dissolution is also likely to occur within the soil porewaters above the caves, where the deposited dust would have much longer timescales to react. Without sampling of rain waters above the actual cave sites using trace-metal clean methods, these two contributions cannot be separated, and in this study both are grouped within the lithogenic weathering sources (see Section 5.1.2).

Drip-water Li/Na ratios are 24 times higher than seawater at Pippikin D and around 2-3 times higher than seawater at the other sites (Table 1). Therefore, marine aerosol inputs can have virtually no influence on the Li budget at Pippikin D and cannot explain the offset in δ^7Li values between local weathering inputs and drip-waters in that location (Fig. 4). Although Pippikin A has lower Li/Na ratios, the similarity of its mean Li isotope composition and temporal evolution to that of Pippikin D (Fig. 4a) is also inconsistent with a marine aerosol influence. Instead, the relatively low Li/Na ratios in Pippikin A could potentially arise from Li removal during uptake by secondary minerals (Section 5.1.3). The drip-waters from White Scar Cave have similar Li/Na ratios to Pippikin A (Table 1) and are probably also minimally affected by marine aerosol inputs. Because seawater has very low Si concentrations, the close relationship between Li and Si concentrations in the drip-waters (Fig. 3c) also argues against a role for marine aerosols in the Li budget of both caves. For the three sites with low Li concentrations, their Si concentrations are around 8 times higher than in the measured rain water (Table 1, Table EA2), while their Si/Na ratios are around 4 times higher than in the measured rain water and 800 times higher than in seawater. We therefore conclude that marine aerosol sources in rain water are a relatively insignificant source of both Si and Li to the cave drip-waters.

5.1.2 Lithogenic weathering sources

The major element chemistry of the drip-waters is broadly consistent with mixing between carbonate and silicate weathering sources, with a greater contribution from carbonates (Fig. 1a). However, the drip-water chemistry also appears to indicate a role for incongruent dissolution and/or the removal of cations (e.g. Mg, Ca) into secondary phases (Fig. 1b), which could comprise clays, oxides, or carbonates. While the Ca budget of the drip-waters is clearly dominated by dissolution of the Great Scar Limestone, the Li content of this limestone is very low and silicate lithologies (e.g. till, shale) are likely to dominate the drip-water Li budget (Table 2, Fig. 5b). A predominant silicate weathering source for Li is supported by the relationships between Li, Na, K, and Si in the drip-waters (Fig. 3), and confirmed by molar Li/Ca ratios, which are 1-2 orders of magnitude higher in the drip-waters (4×10^{-4} for Pippikin D, and $2\text{-}3\times10^{-5}$ for the other sites) (Table 1) than in carbonate leaches of the Great Scar Limestone ($2\text{-}3\times10^{-6}$) (Table EA3). Considering a simplified scenario in which Ca in the drip-waters is entirely derived from the carbonate fraction of the limestone, and where Li and Ca behave conservatively, a simple mass balance indicates a contribution of carbonate weathering to the Li budget of <1 % at Pippikin D (i.e. comparison of Li/Ca ratios between the carbonate leach of the Great Scar Limestone and the drip-waters). Repeating this calculation for the other three sites indicates a slightly higher, but still minor, contribution of carbonate weathering to their Li budgets of ~7-10 %. Note that this calculation ignores removal of Li or Ca from the drip-waters; if there is significant Li removal (relative to Ca), these proportions would be over-estimates of the carbonate weathering contributions. Similar observations have been made for carbonate-dominated river systems, in which minor silicate lithologies almost entirely determine the dissolved Li budget (Kısakűrek et al., 2005).

Among the local silicate sources, we suspect that weathering of the overlying till dominates the Li budget, but we cannot rule out a role for minor shale layers which are reported within Great Scar Limestone (Waltham, 1970) but were not observed to outcrop within either cave in the vicinity of the sampling sites. For Pippikin cave, based on an overlying rock column observed to comprise ~40 m limestone ([Li] = 0.27 μg/g) and ~6 m till ([Li] = 86 μg/g), a mass balance based on Li concentrations would indicate that the Li budget is made up of ~2 % Li contained in the limestone and ~98 % in the silicate-dominated till. For White Scar Cave, considering ~40 m limestone and ~1 m till, ~7 % Li is contained in the carbonate fraction of the limestone ([Li] = 0.12 μg/g based on the carbonate leach) and ~93 % in the silicate sources (i.e. till ([Li] = 37 μg/g) and silicate fraction of the limestone ([Li] = 0.77 μg/g based on difference between bulk limestone and the carbonate leach)). While such first-order estimates of the available Li budget in the lithogenic sources do not address the effects of variable dissolution rates or fluid residence times between rock units, they appear to be in reasonable agreement with our above inferences of carbonate versus silicate contributions based on drip-

water and limestone Li/Ca ratios. In addition, both lines of evidence support the potential for proportionally greater silicate weathering contributions at Pippikin cave than White Scar Cave.

Regardless of the exact partitioning of Li inputs between different silicate sources, or between silicate and carbonate weathering, the major lithogenic sources span a small range of δ^7Li values. Specifically, limestone, shale, till, and cave sediment all have δ^7Li values between -2 ‰ and 0 ‰, with peaty soil only slightly higher at +2 ‰ (Fig. 5a). Therefore, it is not possible to explain either the mean drip-water composition or variability in δ^7Li values from +1 ‰ to +17 ‰ (Fig. 4) simply by mixing between these sources. We rule out the exchangeable fraction in the tills and soils as a major external input or output of the system because its Li content is so low (Table 1). Furthermore, the observation that the bulk till and peaty soil in the vicinity of Pippikin cave differ by only 3 ‰ in δ^7Li values and have similar Li concentrations (slightly lower in the soil) (Table 2) suggests that organics play no major role in the local Li budget, which is fully consistent with findings in previous studies (e.g. Lemarchand et al., 2010; Clergue et al., 2015).

5.1.3 Modification of Li isotopes through uptake by secondary minerals

We demonstrated above that mixing between lithogenic sources is unable to explain the Li isotope compositions of the drip-waters. Therefore, we propose that the input signature of ~-2 to 0 ‰ from primary rock dissolution (Fig. 5a) is significantly modified by the preferential removal of ^{6}Li during secondary mineral formation (e.g. Vigier et al., 2008; Wimpenny et al., 2010; Hindshaw et al., 2019a) or by adsorption onto secondary minerals such as clays or oxides (e.g. Pistiner and Henderson, 2003; Wimpenny et al., 2015; Zhang et al., 2021). Global river water δ^7Li compositions are highly variable with a mean of ~+23 ‰ (Huh et al., 1998; Pogge von Strandmann et al., 2017a), indicating a typical fractionation of more than 20 ‰ from their lithogenic weathering inputs. The operation of a similar process here could therefore explain the range of drip-water compositions from +1 ‰ to +17 ‰, since it would require fractionation in the range of ~2-18 ‰ (mean of ~12 ‰) depending on the degree of Li uptake affecting a given sample.

While the formation of secondary minerals and/or the adsorption of Li onto such minerals is implicated, it is difficult to obtain physical evidence for changes in clay precipitation through time because the amount of clay forming is small relative to the total rock volume (Tipper et al., 2012; Pogge von Strandmann et al., 2019; Golla et al., 2021). In addition, there is the possibility that such fine-grained minerals are transported out of the system in sub-surface water flow (Steinhoefel et al., 2021). However, the formation of such secondary minerals seems feasible based on thermodynamic calculations in PHREEQC (Parkhurst and Appelo, 1999). Using the measured drip-water chemistry and the mean annual surface temperature of 8 °C, these calculations suggest that gibbsite, kaolinite, and Ca-montmorillonite (smectite) are supersaturated, and could therefore form subject to kinetic constraints, while

illite is close to saturation and sometimes supersaturated. For the warmest (16 °C) and coolest (1 °C) months of our study interval, and considering a sample with average drip-water chemistry, the saturation state changes from 3.2 to 5.0 for kaolinite, 1.6 to 2.3 for gibbsite, 0.4 to 2.6 for Ca-montmorillonite (smectite), and -1.5 to 0.6 for illite. Hence, a number of clay minerals appear to be supersaturated over the entire year, with the extent of supersaturation increasing at lower temperatures. Therefore, clay formation in these settings appears feasible. Temporal increases in δ^7Li values also generally correspond to decreasing drip-water Al concentrations, in three out of the four sites (Fig. 6), which could be taken to indicate enhanced removal of Al into secondary minerals such as clays over these intervals.

While the above observations appear consistent with a role for clay formation in Li isotope variability, it is important to emphasise that we do not have any direct evidence for clay formation occurring in the system over the timescales of our observations. Therefore, we cannot evaluate the extent to which amorphous precursors rather than crystalline clays may be forming, and we cannot readily distinguish between Li removal by clay precipitation versus Li adsorption onto existing clay minerals (although these two processes are generally associated with different fractionation factors; see Section 5.3). In addition, the formation of other phases such as Fe oxides/oxyhydroxides could also represent a viable sink of light Li isotopes (Pistiner and Henderson, 2003; Steinhoefel et al., 2021).

5.2 Controls on temporal variations in Li isotopes

Temporal variability in drip-water Li isotopes indicates rapid changes in weathering processes over monthly to seasonal timescales (Fig. 4). As discussed above, the source inputs are uniform in Li isotope composition (δ^7Li ~-2 to 0 ‰; Fig. 5) and secondary mineral formation (or adsorption onto such minerals) is likely required to drive the drip-water Li isotopes to higher values. Therefore, changes through time in the relative balance of silicate rock dissolution versus secondary mineral formation, or in the isotopic fractionation factor during secondary mineral formation, may have been a major driver of drip-water Li isotope variability. In this section, we use records of temperature, precipitation, drip-water chemistry, and drip rates to address the controls on the Li isotope changes and their implications for weathering processes.

5.2.1 Temperature-dependent isotope fractionation

The isotopic fractionation of Li between fluids and secondary minerals such as clays is temperature-dependent (Vigier et al., 2008; Li and West, 2014; Dupuis et al., 2017), which leads to the potential for seasonal temperature changes to influence the fluid composition independent of changes in weathering processes (Gou et al., 2019). Although the isotopic fractionation may also depend on the exact minerology of the secondary minerals, a similar temperature-dependence has been reported in both laboratory experiments on clays and in

natural settings (with presumably mixed assemblages of secondary minerals), with fractionation decreasing by ~0.18 ‰ per 1°C of warming over the temperature range of ~0-30 °C (Li and West, 2014; Gou et al., 2019).

Warmer temperatures during summer would be expected to generate less isotopic fractionation, leading to lower (i.e. less fractionated) δ^7Li values in the weathering fluids. Assuming that a significant proportion of Li is removed from the fluids by an equilibrium (or batch) process, and additionally making the simplification that seasonal variations of ~10 °C in mean monthly surface temperatures (Fig. 7a) are relevant to the depths where weathering is occurring, such an effect could potentially lower peak summer drip-water δ^7Li compositions by up to 1.8 ‰ over peak winter values. In contrast, the observations indicate generally higher δ^7Li values during summer (Table 1, Fig. 7a). Therefore, temperature-dependent fractionation does not seem able to explain the variation seen in our records. By working in the opposite direction, it could potentially even lead to a more muted Li isotope response in the drip-waters than the true weathering signal. However, applying a temperature correction to each drip-water sample (using the monthly temperature data and otherwise the same assumptions as above) would only increase the magnitude of the seasonal difference in mean drip-water δ^7Li values (i.e. March-August minus September-February) from the measured +3.0 ‰ to +3.7 ‰. Therefore, since temperature variations appear capable of exerting only a minor direct influence on the isotopic fractionation, we do not consider this effect further.

5.2.2 Fluid source changes

There is no clear link between precipitation amounts and drip-water Li isotopes (Fig. 7c), which is consistent with marine aerosols in rain water providing only a minor source of Li to the drip-waters. However, any rainfall source signal may be delayed during transport through the epikarst (Bottrell and Atkinson, 1992), so we also use stable oxygen isotopes (δ^{18}O) in the cave drip-waters as a signal of changes in the precipitation source and/or amount (Fairchild and Baker, 2012), while recognising that modification of that signal is possible within the sub-surface (Treble et al., 2013). Regardless of the exact controls on drip-water δ^{18}O values, there is also no direct link between the Li isotope changes and the δ^{18}O records (Fig. 7d). In particular, during winter 2016 to spring 2017, it is clear that drip-water δ^{18}O values shifted towards lower values a few months before the major Li isotope shift occurred (Fig. 7d). Therefore, changing precipitation inputs do not appear to exert a direct control on the drip-water Li isotope records.

An alternative fluid source effect could potentially arise indirectly from changes in precipitation, because changes in the water balance could affect fluid pathways and timescales, and therefore change the sources of water influencing a given drip-water site (Bottrell and Atkinson, 1992; McDonald et al., 2007). Since all potential lithogenic input sources have similar Li isotope compositions in both cave settings (Fig. 5a), a switch in fluid pathways that

changes the proportions of Li derived from weathering of different lithologies should have no significant effect on drip-water Li isotopes. However, variability in precipitation (and hence effective precipitation) could change the water residence time in the sub-surface and/or lead to mixing between local sub-surface reservoirs with different storage times. The implications of such changes could also differ between different isotopic systems, and we return to this hypothesis in Section 5.2.4.

5.2.3 Temperature-dependent weathering kinetics

Seasonal temperature changes could potentially have a major influence on weathering processes, and specifically the weathering congruence (Pogge von Strandmann et al., 2014; Pogge von Strandmann et al., 2017c). Such a situation could arise because increased temperatures may promote faster kinetics for silicate mineral dissolution (Gislason et al., 2009; Eiriksdottir et al., 2013), while decreasing the saturation state and increasing the solubility of non-oxide secondary minerals such as clays (Pokrovski et al., 1998; Stefánsson and Gíslason, 2001). Therefore, warm conditions could enhance the dissolution of primary silicate minerals within the till and soil, while hindering modification by secondary mineral formation, leading to low dissolved δ^7Li compositions in the drip-waters. As temperature decreases, the extent of oversaturation of kaolinite and Ca-montmorillonite in the cave drip-waters increases (Section 5.1.3), while illite may also become slightly oversaturated in the coolest months. Therefore, cooler conditions could reduce the dissolution of silicates, while decreasing the solubility of (non-oxide) secondary minerals thereby increasing their stability (Pokrovski et al., 1998; Stefánsson and Gíslason, 2001), which would enhance Li removal and generate higher δ^7Li compositions.

The observation of generally higher drip-water Li isotope compositions during spring and summer (Fig. 7a) does not initially appear consistent with the above mechanism. However, the most prominent shift from low to high δ^7Li values occurred during late winter 2016 to spring 2017 (i.e. November 2016 to April 2017), during an interval when temperatures were low (Fig. 7a). Therefore, while δ^7Li values were generally higher during summer, the shifts towards these values typically occurred within the preceding winter. Comparing the mean δ^7Li values for each cave with an inverted temperature curve could support such a control of temperature on the balance between rock dissolution and clay formation, but with a lag behind atmospheric temperatures of around 3-6 months (Fig. 7b).

A lagged response of the weathering signal to changes in surface air temperature might be expected, due to (i) the time needed for temperatures in the weathering system to respond to changes in atmospheric temperatures; (ii) the time needed for changes in weathering reactions (e.g. clay or oxide precipitation, or ion exchange) to occur and progress sufficiently to influence the porewater Li isotopes; and (iii) the time needed for water to flow from the soil porewaters (where most of the silicate weathering is probably occurring) to the cave drip-water

sites. The Mg, Sr, and B contents of the drip-waters (and their ratios to Na) also display a seasonal cycle with a lag behind air temperatures, but the lag is only ~2 months (Fig. 2), similar to the lag between air temperatures and drip-water $\delta^{18}O$ changes (Fig. 7a,d). Elevated Mg, Sr, and B concentrations during summer likely arise from some combination of increases in soil leaching contributions (McDonald et al., 2007) and/or increases in prior calcite precipitation (Fairchild et al., 2000). Hence, these chemical data could be explained by a fast response of such processes to climate in combination with a mean timescale of 1-2 months for water transport to the sampling sites, consistent with previous studies of tracer transport in the White Scar Cave system (Bottrell and Atkinson, 1992).

If temperature changes are to be invoked to explain the Li isotope variability, an additional lag of several months appears to be required for Li isotopes compared to those trace element (Mg, Sr, B) and hydrographic ($\delta^{18}O$) records (Fig. 7). We cannot rule out that some of the secondary mineral formation (or adsorption onto those minerals) may be occurring at depth within limestone pore spaces and fractures, rather than in the till and soils, in which case there may be a significant lag in the seasonal temperature response in the weathering zone compared to the atmosphere (Rau et al., 2015). Alternatively, a slower response time for silicate weathering could arise from the kinetics of secondary mineral nucleation and growth, which for clays may be relatively slow at these temperatures (Hindshaw et al., 2019a), although presumably it would be accelerated if amorphous phases are forming under supersaturated conditions. Since it is challenging to transfer reaction rates between laboratory and field settings, we instead note that field data from a recent study demonstrated that Mg-rich secondary minerals can form and impact upon the major element chemistry of solutions within 1–2 months at low temperatures (Oelkers et al., 2019). Therefore, secondary clay formation over seasonal timescales in the soil porewaters and cave drip-waters appears a feasible possibility.

Overall, the relationship between changes in atmospheric temperatures and drip-water $\delta^{7}Li$ values supports a possible control of silicate weathering kinetics on seasonal changes in Li removal and isotope fractionation, but with lags in the response to temperature of several months (Fig. 7b). However, at present, fluid transport timescales in the system are too poorly constrained to fully evaluate the temperature control on the reactions, while the sampling interval is too similar to the timescales of interest to evaluate the possible cause(s) of the apparently lagged response between different geochemical tracers. In future, higher-resolution sampling could perhaps provide better insight into such processes that are operating and the response time of the weathering system.

5.2.4 Fluid residence time

While temperature changes could play some role in determining the balance between silicate dissolution and clay formation, any such relationship is clearly complex. Instead, or in

addition, reactive transport models suggest a control on Li isotopes could arise from changes in fluid residence time in the soils and/or limestone system (Lemarchand et al., 2010; Maher, 2010; Wanner et al., 2014; Wanner et al., 2017). Specifically, increases in fluid residence time during dry intervals could enhance secondary clay formation, leading to increased Li removal and higher drip-water δ^7Li values, whereas faster transport during wet intervals could hinder secondary clay formation, leading to less fractionated δ^7Li values.

We test this idea by comparing the Li isotope records from Pippikin A and Pippikin D to instantaneously monitored drip rates during sample collection for Pippikin A (Fig. 8a) and to a monthly-smoothed record of drip rates in the same cave chamber as Pippikin D (Fig. 8b). For Pippikin A, there is a close agreement between instantaneous drip rates and drip-water δ^7Li values, with higher δ^7Li values linked to lower drip rates (Fig. 8a). For Pippikin D, monthly to seasonal shifts towards higher δ^7Li values also correspond to intervals with decreasing drip rates, although the link appears stronger with the monthly-smoothed data from the "Stalagmate" drip logger (Fig. 8b) than with the instantaneous measurements (Table 1). For the latter, the drip rates of three samples appear anomalously higher and may not be representative. In addition, an underlying long-term trend from 2016 to 2018 is seen in both the Li isotope and drip rate records from Pippikin cave, with an increase in δ^7Li values corresponding to a decline in drip rates (Fig. 8). Based on the assumption that fluid residence time is inversely related to drip rates over such timescales, these data support a clear role for fluid residence time in determining the balance between silicate dissolution and clay formation.

In contrast to the observations in Pippikin cave (Fig. 8), we do not resolve a link between instantaneous drip rates and Li isotopes at the White Scar Cave drip sites (Table 1). This observation could suggest that temperature (Fig. 7a,b) rather than fluid residence time is a stronger control in White Scar Cave. However, we are cautious of over-interpreting this observation, because the more continuous nature of the White Scar Cave drips may not provide constraints on the fluid residence time in this system. In addition, we caution that drip rates and fluid pathways can vary significantly, even between adjacent drip sites under identical climate forcing (Bottrell and Atkinson, 1992; Roberts et al., 1999). While such local differences in fluid pathways and residence times between drip-water sites could lead to inter-site and inter-cave variability in Li isotopes (Fig. 4), higher resolution sampling of Li isotopes and drip rates would be needed to directly evaluate this effect. Quantifying the relative contributions of temperature-dependent kinetics and changes in fluid residence times to seasonal changes in weathering processes and Li isotopes is beyond the capability of our present dataset and would appear to be an important future research goal.

5.3 Quantification of Li removal into secondary minerals

To provide further first-order constraints on weathering processes in these systems, we use the drip-water Li isotope compositions to estimate the proportion of Li that has been removed into secondary minerals. We assume that dissolved Li is dominantly derived from the weathering of silicates in the till and/or shale layers, with a δ^7Li composition of -1 ± 1 ‰ (yellow band in Fig. 5a), and calculate Li removal using an equilibrium (or batch) fractionation model. Such a model has previously been proposed to explain both the weathering of regolith in the Amazon basin (Maffre et al., 2020) and global-scale river chemistry (Pogge von Strandmann et al., 2017a). While recognising that the exact nature of the secondary phases is unconstrained, we follow previous studies in using fractionation factors for secondary clays. The experimentally-determined fractionation between fluid and clays (stevensite and saponite) is 16.6 ± 1.7 ‰ (2sd) at 20 °C (Hindshaw et al., 2019a), which would translate to ~17-20 ‰ at the mean annual temperature of our sites (8 °C) (Li and West, 2014; Gou et al., 2019). Hence, the range of fractionation required to explain our drip-water dataset (i.e. ~1-19 ‰, average ~12 ‰) can be achieved by clay formation via equilibrium (batch) fractionation.

Using a batch model with a fractionation factor ($\alpha_{clay\text{-}fluid}$) of 0.9815 (Li and West, 2014; Gou et al., 2019; Hindshaw et al., 2019a), the average Pippikin cave Li isotope data could be explained by removal of ~60 % of the initial Li, while the average White Scar Cave data could be explained by removal of ~70 %. Furthermore, the seasonal shift in Li isotope compositions between November 2016 and April 2017 (Fig. 7b) would imply enhanced Li removal by secondary clay formation during winter, increasing from ~50 % to ~70 % in Pippikin cave and from ~50 % to ~80 % in White Scar Cave. Interestingly, these seasonal changes are comparable in both direction and magnitude to estimates of glacial-interglacial changes from Li isotopes in two speleothems from Israel, where Li removal from the drip-waters was inferred to have increased from ~50 % during warm interglacials to ~70 % during cool glacials (Pogge von Strandmann et al., 2017c). While cautioning against a direct comparison because the speleothem study used a Rayleigh fractionation model (Pogge von Strandmann et al., 2017c), the two studies appear to indicate a broadly similar response of Li removal to temperature changes of ~10℃, thereby supporting either a direct or indirect temperature control on weathering processes.

Following an approach taken in studies on river waters (e.g. Lemarchand et al., 2010; Liu et al., 2015; Manaka et al., 2017; Pogge von Strandmann et al., 2017a), we also attempt to model the Li isotope evolution in combination with Li/Na ratios. The formation of clays or oxides is expected to remove Li while leaving Na largely unaffected, because Na is generally a mobile major cation (Gislason et al., 1996), such that Li/Na ratios should decrease with increasing secondary mineral formation. As above, we use a Li isotope composition for the initial fluid based on local silicate sources (i.e. till, soils, shale) (Fig. 5) and model isotopic fractionation using a batch model and a fractionation factor of 0.9815 based on clays (Li and West, 2014; Gou et al., 2019; Hindshaw et al., 2019a) (Fig. 9). The general pattern of the data

can be explained by such a model, indicating relatively more silicate dissolution at Pippikin D (low δ^7Li and high Li/Na) and more clay formation at Pippikin A and the White Scar Cave sites (higher δ^7Li and low Li/Na) (Fig. 9a). However, when using the Li/Na ratios of the local silicate sources to constrain the initial fluid composition, the drip-water data fall significantly below the fractionation lines (Fig. 9a). Since the local rocks and till may not weather congruently, and could contain relatively unreactive Li-rich secondary clays that are the product of weathering reactions (e.g. Lemarchand et al., 2010), we also explore a fractionation model starting from the Li/Na ratios of the upper continental crust (Rudnick and Gao, 2003; Teng et al., 2004) (Fig. 9b). This latter approach may better represent the inputs from primary mineral dissolution within the till, and in this case there is a much closer fit to the data, but it is still not possible to simultaneously fit the Pippikin D data and all the data from the other sites with the same model parameters (Fig. 9b). In particular, it is hard to explain the Li isotope data linked to low Li/Na ratios at the other sites, while an even poorer fit would be achieved using a Rayleigh fractionation model (Fig. 9b).

The apparent decoupling between Li isotopes and Li concentrations (or Li/Na ratios) in the cave drip-waters (Fig. 9) could indicate the complexity of cave systems in comparison to river systems. Nevertheless, it is important to recognise that rivers also record significant variability, rather than a single universal δ^7Li-Li/Na relationship (Millot et al., 2010b; Murphy et al., 2019). One possible complication in caves is that Li could be supplied from local fluid reservoirs with different initial Li/Na ratios, leading to data falling along individual fractionation paths. Another possibility is that the weathering of glacial tills produces a more complex relationship between δ^7Li and Li/Na ratios, as proposed for glacially-ground sediments in the Mackenzie River (Millot et al., 2010b). However, neither mechanism would seem that likely to explain the differences between data from Pippikin A and Pippikin D within the same cave system (Fig. 9).

A more viable option for decoupling between Li isotopes and Li/Na ratios is a multi-step evolution involving mixing between multiple fluid reservoirs (Fig. 9c). For example, for waters that have evolved to high δ^7Li values and low Li/Na ratios, a subsequent mixing event could introduce Li from a less evolved reservoir that has a composition closer to the original source composition (i.e. low δ^7Li values and high Li/Na ratios). Such a scenario (red arrow in Fig. 9c) could help explain why some samples from Pippikin A and White Scar Cave fall below the modelled batch fractionation line. This mechanism appears feasible given the evidence for multiple fluid pathways leading to different fluid residence times in the unsaturated zone of White Scar Cave (Bottrell and Atkinson, 1992), but it is hard to fully evaluate because fluid residence times in the soil layers are unconstrained and residence times in the caves likely vary in a complex manner through space and time (Fig. 8).

Alternatively, or in addition, changes in Li adsorption onto pre-existing clay minerals could also be occurring, and could be decoupled in space and/or time from secondary clay

formation. Indeed, such exchange processes have been proposed to control porewater Mg cycling (Fries et al., 2019), although evidence for an important effect of the exchangeable fraction on Li isotope budgets has so far been mostly lacking (e.g. Pogge von Strandmann et al., 2019). Whereas secondary clay formation involves large isotopic fractionation factors due to structural Li incorporation into the octahedral sites, the removal of Li by ion exchange typically generates less isotopic fractionation, depending on factors such as the clay mineralogy, the specific adsorption site, and the solution chemistry (Pistiner and Henderson, 2003; Huh et al., 2004; Wimpenny et al., 2015; Hindshaw et al., 2019a; Pogge von Strandmann et al., 2019; Zhang et al., 2021). In particular, it has been shown that Li isotopic fractionation can be large in the case of adsorption as octahedral inner-sphere complexes (e.g. Zhang et al., 2021), but is virtually absent in the case of outer-sphere complexation of Li with 4-fold coordination in the clay interlayers (e.g. Hindshaw et al., 2019a). Interestingly, the exchangeable fractions in the Pippikin till and soil (Table 2) had fairly similar δ^7Li values to the cave drip-waters (Fig. 4), which suggests that any Li removal into such fractions did not involve a large isotopic fractionation. It follows that if Li is removed by both clay precipitation (with a large fractionation) and by adsorption/exchange (with a smaller fractionation), and if those processes operate independently, then Li isotopes and concentrations could become decoupled, enabling data points to fall below the modelled batch fractionation trend (Fig. 9c). Finally, we note that, in the context of a system with at least three potential removal mechanisms for Li (i.e. clay precipitation, interlayer exchange, and oxide formation), and where seasonal or shorter timescales are considered, the inability to fit the data by a single batch or Rayleigh model probably in part reflects non-steady state behaviour (Steinhoefel et al., 2021).

5.4 Implications for weathering processes

While fully quantitative interpretations of the Li isotope data are not possible, this study provides intriguing evidence for temporal changes in the balance between rock dissolution and secondary mineral formation (Figs. 6 and 9). Furthermore, the inferred control exerted by variations in fluid residence time (Fig. 8) is consistent with recent observations of Li isotope behaviour in rivers and soils. For example, studies on river systems with distinct wet and dry seasons have proposed that higher dissolved δ^7Li values during times of low flow arise from longer fluid residence times and increased secondary clay formation (Liu et al., 2015; Manaka et al., 2017; Hindshaw et al., 2019b), while a similar control has previously been invoked to explain seasonality in river water Mg isotopes (Tipper et al., 2012). A study from Guadeloupe has also suggested that a decrease in fluid residence time can lead to lower δ^7Li values in groundwater, invoking suppressed secondary mineral formation following a heavy rainfall event (Fries et al., 2019). Since the tropical climate, highly weathered andesitic bedrock, and

shallow hydrological setting of that study were quite different from the Yorkshire cave setting, the combination of observations from these two contrasting systems appears to indicate a general control of fluid residence time on the weathering system.

Studies of river water chemistry can record complex and/or smoothed signals of temporal changes in weathering due to mixing between individual tributaries (e.g. Henchiri et al., 2016) or between different reservoirs (e.g. runoff, soil porewaters, deep groundwater). In contrast, our observations and those of Fries et al. (2019) confirm the potential for rapid temporal variability in weathering processes and weathering signatures within soil porewater and/or shallow groundwater systems. Therefore, monthly to seasonal changes in water-rock interaction within soil porewaters or fractured bedrock may exert a significant control on the Li isotope compositions of the inputs to rivers and hence on riverine compositions. Future studies may explore these processes further using cave drip-waters as a means to generate high-resolution time series of soil porewater Li isotopes in multiple settings and over a range of timescales. Such evidence would inform on both interpretations of the Li isotope proxy, and the potential for rapid changes in chemical weathering processes in response to changes in hydrology or climate.

Unlike the effect of fluid residence times, a temperature control on weathering kinetics (Fig. 7b) has not previously been demonstrated using Li isotopes in large river systems. However, research on small local systems may better allow the response of weathering to temperature changes to be isolated, without overprinting from changes in mixing and transport. Studies on soil chronosequences (Ryu et al., 2014) and speleothems (Pogge von Strandmann et al., 2017c) have both suggested that warmer temperatures can lead to more congruent weathering with less secondary clay formation, while cooler conditions allow more retention of cations and Li in secondary minerals, which is supported by thermodynamic data (Pokrovski et al., 1998). By identifying a link between seasonal temperature variations and the extent of Li removal from soil porewaters, particularly in samples from White Scar Cave, our results appear to support those studies, and further suggest they may be extended over seasonal or shorter timescales. However, our interpretations of the drip-water data are limited by a lack of constraints on subsurface fluid pathways and residence times, and there are several mechanisms that could potentially generate a lagged response in the Li isotope signature relative to climate forcing. In addition, the specific mechanisms (precipitation, adsorption, or cation exchange) and mineralogy (clays, amorphous phases, or oxides) influencing our Li isotope data also remain uncertain, and therefore we urge some caution in how such data are interpreted over these shorter timescales.

Finally, we emphasise that temporal changes in secondary clay formation would translate into changes in weathering efficiency that could influence carbon dioxide drawdown. Specifically, intervals with colder temperatures and/or longer subsurface fluid residence times might lead to proportionally more secondary clay formation, reducing the efficiency of carbon sequestration by weathering. The opposite situation could arise during intervals with warmer

temperatures and/or shorter fluid residence times, since more congruent weathering (i.e. increased primary mineral dissolution relative to secondary clay formation) could lead to more efficient carbon drawdown. Therefore, rather than simply responding to the mean global climate state, it appears that future weathering changes could be sensitive to variability in local hydrographic conditions linked to an increased prevalence of extreme weather events such as storms (Mölter et al., 2016) and droughts (Samaniego et al., 2018). In such a scenario, both increased primary rock dissolution and enhanced weathering efficiency (due to reduced secondary mineral formation), in combination, might be expected to contribute to increased carbon dioxide drawdown by silicate weathering. However, quantifying the regional or global scale weathering response to such changes will require improved constraints on the controls on weathering processes, and on how they are recorded by systems such as Li isotopes as a function of secondary mineralogy, over a range of spatial and temporal scales. Since the Li isotope signal in cave drip-waters reflects silicate weathering in the overlying soils, speleothems from well-constrained systems could provide a useful archive of the local response of Li isotopes, and potentially silicate weathering processes, to climate changes over longer timescales.

6. Conclusions

Monitoring of drip-water Li isotopes in two Yorkshire caves reveals complex spatial and temporal variability that suggests a link between climate forcing and weathering processes in soil porewaters on monthly to seasonal timescales. Specifically, our data demonstrate that temperature and fluid residence time appear to exert controls on drip-water δ^7Li values, likely reflecting changes in the extent of Li removal into secondary minerals. Because of the differing controls on primary mineral dissolution and secondary mineral formation, cooler temperatures and/or longer fluid residence times may lead to enhanced secondary mineral formation relative to rock dissolution, leading to higher drip-water δ^7Li values. If the secondary minerals are clays, this scenario could represent a significant reduction in weathering efficiency, because secondary clay formation reduces the efficiency of carbon dioxide drawdown from silicate weathering. However, at present, we cannot rule out alternative controls from adsorption or exchange of Li with existing mineral surfaces, or a contribution from oxides rather than clays; in these latter cases, the impact on weathering efficiency would likely be smaller.

Our results have two broader implications. First, the variability in Li isotopes over short temporal and spatial scales should be considered when interpreting paleo-records of Li isotopes in terms of changes in weathering processes or intensity. Second, our Li isotope evidence suggests that both past and future weathering changes may be sensitive to seasonality or to extreme weather events that influence the local hydrological cycle, rather than responding only to the mean global climate state. More intense rainfall events in future might be expected to lead to both increased primary rock dissolution and enhanced weathering efficiency (due to

reduced clay formation), thereby increasing carbon dioxide drawdown by silicate weathering, but such a hypothesis is presently speculative and needs to be tested with further experimental data and field data from a wider range of settings.

Acknowledgments

This study and DJW, PPvS, and GT were funded by ERC Consolidator grant 682760 CONTROLPASTCO2. DJW is currently supported by a NERC independent research fellowship (NE/T011440/1). We are grateful to three anonymous reviewers, whose detailed comments helped us to significantly improve the manuscript, and to the associate editor Brian Stewart for his thoughtful input.

References

Aitkenhead N., Barclay W.J., Brandon A., Chadwick R.A., Chisholm J.I., Cooper A.H., Johnson E.W. (2002) *British Regional Geology: the Pennines and adjacent areas, 4th edition*. British Geological Survey, Nottingham.

Andrews J.T., King C.A.M. (1968) Comparative till fabrics and till fabric variability in a till sheet and a drumlin: a small-scale study. *Proceedings of the Yorkshire Geological Society* **36**, 435-461.

Berner R.A., Lasaga A.C., Garrels R.M. (1983) The carbonate-silicate geochemical cycle and its effect on atmospheric carbon dioxide over the past 100 million years. *Am. J. Sci.* **283**, 641-683.

Bottrell S.H., Atkinson T.C. (1992) Tracer study of flow and storage in the unsaturated zone of a karstic limestone aquifer, in: Hötzl H., Werner, A. (Ed.), *Tracer Hydrology, Proceedings of the 6th International Symposium on Water Tracing, Karlsruhe, Germany, 21-26 September 1992*. Balkema, Rotterdam, pp. 207-211.

Burt T.P., Horton B.P. (2003) The climate of Malham Tarn. *Field Studies* **10**, 635-652.

Calmels D., Galy A., Hovius N., Bickle M., West A.J., Chen M.-C., Chapman H. (2011) Contribution of deep groundwater to the weathering budget in a rapidly eroding mountain belt, Taiwan. *Earth Planet. Sci. Lett.* **303**, 48-58.

Clauer N., Williams L.B., Lemarchand D., Florian P., Honty M. (2018) Illitization decrypted by B and Li isotope geochemistry of nanometer-sized illite crystals from bentonite beds, East Slovak Basin. *Chemical Geology* **477**, 177-194.

Clergue C., Dellinger M., Buss H.L., Gaillardet J., Benedetti M.F., Dessert C. (2015) Influence of atmospheric deposits and secondary minerals on Li isotopes budget in a highly weathered catchment, Guadeloupe (Lesser Antilles). *Chemical Geology* **414**, 28-41.

Dellinger M., Gaillardet J., Bouchez J., Calmels D., Louvat P., Dosseto A., Gorge C., Alanoca L., Maurice L. (2015) Riverine Li isotope fractionation in the Amazon River basin controlled by the weathering regimes. *Geochim. Cosmochim. Acta* **164**, 71-93.

Dellinger M., Hardisty D.S., Planavsky N.J., Gill B.C., Kalderon-Asael B., Asael D., Croissant T., Swart P.K., West A.J. (2020) The effects of diagenesis on lithium isotope ratios of shallow marine carbonates. *Am. J. Sci.* **320**, 150-184.

930 Dupuis R., Benoit M., Tuckerman M.E., Meheut M. (2017) Importance of a fully anharmonic
931 treatment of equilibrium isotope fractionation properties of dissolved ionic species as
932 evidenced by Li^+ (aq). *Accounts of Chemical Research* **50**, 1597-1605.
933 Eiriksdottir E.S., Gislason S.R., Oelkers E.H. (2013) Does temperature or runoff control the
934 feedback between chemical denudation and climate? Insights from NE Iceland.
935 *Geochim. Cosmochim. Acta* **107**, 65-81.
936 Fairchild I.J., Borsato A., Tooth A.F., Frisia S., Hawkesworth C.J., Huang Y., McDermott F.,
937 Spiro B. (2000) Controls on trace element (Sr–Mg) compositions of carbonate cave
938 waters: implications for speleothem climatic records. *Chemical Geology* **166**, 255-269.
939 Fairchild I.J., Baker A. (2012) *Speleothem science: from process to past environments*.
940 Wiley-Blackwell.
941 Fries D.M., James R.H., Dessert C., Bouchez J., Beaumais A., Pearce C.R. (2019) The
942 response of Li and Mg isotopes to rain events in a highly-weathered catchment.
943 *Chemical Geology* **519**, 68-82.
944 Gaillardet J., Dupre B., Louvat P., Allegre C.J. (1999) Global silicate weathering and CO_2
945 consumption rates deduced from the chemistry of large rivers. *Chemical Geology* **159**, 3-
946 30.
947 Gislason S.R., Arnorsson S., Armannsson H. (1996) Chemical weathering of basalt in
948 Southwest Iceland; effects of runoff, age of rocks and vegetative/glacial cover. *Am. J.*
949 *Sci.* **296**, 837-907.
950 Gislason S.R., Oelkers E.H., Eiriksdottir E.S., Kardjilov M.I., Gisladottir G., Sigfusson B.,
951 Snorrason A., Elefsen S., Hardardottir J., Torssander P., Oskarsson N. (2009) Direct
952 evidence of the feedback between climate and weathering. *Earth Planet. Sci. Lett.* **277**,
953 213-222.
954 Golla J.K., Kuessner M.L., Henehan M.J., Bouchez J., Rempe D.M., Druhan J.L. (2021) The
955 evolution of lithium isotope signatures in fluids draining actively weathering hillslopes.
956 *Earth Planet. Sci. Lett.* **567**, 116988.
957 Gou L.-F., Jin Z., Pogge von Strandmann P.A.E., Li G., Qu Y.-X., Xiao J., Deng L., Galy A.
958 (2019) Li isotopes in the middle Yellow River: Seasonal variability, sources and
959 fractionation. *Geochim. Cosmochim. Acta* **248**, 88-108.
960 Gou L.F., Liu C.Y., Deng L., Jin Z. (2020) Quantifying the impact of recovery during
961 chromatographic purification on the accuracy of lithium isotopic determination by MC-
962 ICP-MS. *Rapid Communications in Mass Spectrometry*, 34:e8577, doi:
963 10.1002/rcm.8577.
964 Hathorne E.C., James R.H. (2006) Temporal record of lithium in seawater: A tracer for
965 silicate weathering? *Earth Planet. Sci. Lett.* **246**, 393-406.
966 Heimburger A., Tharaud M., Monna F., Losno R., Desboeufs K., Nguyen E.B. (2013) SLRS-
967 5 elemental concentrations of thirty-three uncertified elements deduced from SLRS-
968 5/SLRS-4 ratios. *Geostandards and Geoanalytical Research* **37**, 77-85.
969 Henchiri S., Gaillardet J., Dellinger M., Bouchez J., Spencer R.G.M. (2016) Riverine
970 dissolved lithium isotopic signatures in low-relief central Africa and their link to
971 weathering regimes. *Geophys. Res. Lett.* **43**, 4391-4399.
972 Hindshaw R.S., Tosca R., Goût T.L., Farnan I., Tosca N.J., Tipper E.T. (2019a) Experimental
973 constraints on Li isotope fractionation during clay formation. *Geochim. Cosmochim.*
974 *Acta* **250**, 219-237.

Hindshaw R.S., Teisserenc R., Le Dantec T., Tananaev N. (2019b) Seasonal change of geochemical sources and processes in the Yenisei River: A Sr, Mg and Li isotope study. *Geochim. Cosmochim. Acta* **255**, 222-236.

Huh Y., Chan L.-H., Zhang L., Edmond J.M. (1998) Lithium and its isotopes in major world rivers: implications for weathering and the oceanic budget. *Geochim. Cosmochim. Acta* **62**, 2039-2051.

Huh Y., Chan L.-H., Edmond J.M. (2001) Lithium isotopes as a probe of weathering processes: Orinoco River. *Earth Planet. Sci. Lett.* **194**, 189-199.

Huh Y., Chan L.H., Chadwick O.A. (2004) Behavior of lithium and its isotopes during weathering of Hawaiian basalt. *Geochemistry, Geophysics, Geosystems* **5**, doi: 10.1029/2004GC000729.

James R.H., Palmer M.R. (2000) The lithium isotope composition of international rock standards. *Chemical Geology* **166**, 319-326.

Jeffcoate A.B., Elliott T., Thomas A., Bouman C. (2004) Precise/small sample size determinations of lithium isotopic compositions of geological reference materials and modern seawater by MC-ICP-MS. *Geostandards and Geoanalytical Research* **28**, 161-172.

Jochum K.P., Weis U., Schwager B., Stoll B., Wilson S.A., Haug G.H., Andreae M.O., Enzweiler J. (2016) Reference values following ISO guidelines for frequently requested rock reference materials. *Geostandards and Geoanalytical Research* **40**, 333-350.

Kısakűrek B., James R.H., Harris N.B.W. (2005) Li and δ^7Li in Himalayan rivers: proxies for silicate weathering? *Earth Planet. Sci. Lett.* **237**, 387-401.

Krissansen-Totton J., Catling D.C. (2017) Constraining climate sensitivity and continental versus seafloor weathering using an inverse geological carbon cycle model. *Nature Communications* **8, 15423**, doi: 10.1038/ncomms15423.

Lemarchand E., Chabaux F., Vigier N., Millot R., Pierret M.-C. (2010) Lithium isotope systematics in a forested granitic catchment (Strengbach, Vosges Mountains, France). *Geochim. Cosmochim. Acta* **74**, 4612-4628.

Li G., West A.J. (2014) Evolution of Cenozoic seawater lithium isotopes: Coupling of global denudation regime and shifting seawater sinks. *Earth Planet. Sci. Lett.* **401**, 284-293.

Li G., Hartmann J., Derry L.A., West A.J., You C.-F., Long X., Zhan T., Li L., Li G., Qiu W. (2016) Temperature dependence of basalt weathering. *Earth Planet. Sci. Lett.* **443**, 59-69.

Liu X.-M., Rudnick R.L., McDonough W.F., Cummings M.L. (2013) Influence of chemical weathering on the composition of the continental crust: Insights from Li and Nd isotopes in bauxite profiles developed on Columbia River Basalts. *Geochim. Cosmochim. Acta* **115**, 73-91.

Liu X.-M., Wanner C., Rudnick R.L., McDonough W.F. (2015) Processes controlling δ^7Li in rivers illuminated by study of streams and groundwaters draining basalts. *Earth Planet. Sci. Lett.* **409**, 212-224.

Livingstone S.J., Evans D.J.A., Ó Cofaigh C., Davies B.J., Merritt J.W., Huddart D., Mitchell W.A., Roberts D.H., Yorke L. (2012) Glaciodynamics of the central sector of the last British–Irish Ice Sheet in Northern England. *Earth-Sci. Rev.* **111**, 25-55.

Maffre P., Goddéris Y., Vigier N., Moquet J.-S., Carretier S. (2020) Modelling the riverine δ^7Li variability throughout the Amazon Basin. *Chemical Geology*, 119336, doi: 10.1016/j.chemgeo.2019.119336.

Maher K. (2010) The dependence of chemical weathering rates on fluid residence time. *Earth Planet. Sci. Lett.* **294**, 101-110.

Manaka T., Araoka D., Yoshimura T., Hossain H.Z., Nishio Y., Suzuki A., Kawahata H. (2017) Downstream and seasonal changes of lithium isotope ratios in the Ganges-Brahmaputra river system. *Geochemistry, Geophysics, Geosystems* **18**, 3003-3015.

McDonald J., Drysdale R., Hill D., Chisari R., Wong H. (2007) The hydrochemical response of cave drip waters to sub-annual and inter-annual climate variability, Wombeyan Caves, SE Australia. *Chemical Geology* **244**, 605-623.

Millot R., Petelet-Giraud E., Guerrot C., Négrel P. (2010a) Multi-isotopic composition (δ^7Li–δ^{11}B–δD–δ^{18}O) of rainwaters in France: Origin and spatio-temporal characterization. *Appl. Geochem.* **25**, 1510-1524.

Millot R., Vigier N., Gaillardet J. (2010b) Behaviour of lithium and its isotopes during weathering in the Mackenzie Basin, Canada. *Geochim. Cosmochim. Acta* **74**, 3897-3912.

Misra S., Froelich P.N. (2012) Lithium isotope history of Cenozoic seawater: changes in silicate weathering and reverse weathering. *Science* **335**, 818-823.

Mitchell W.A. (1991) Dimlington Stadial ice sheet in the western Pennines, in: Mitchell W.A. (Ed.), *Western Pennines: Field Guide*. Quaternary Research Association, London, pp. 25-42.

Mitchell W.A. (1994) Drumlins in ice sheet reconstructions, with reference to the western Pennines, northern England. *Sediment. Geol.* **91**, 313-331.

Mölter T., Schindler D., Albrecht A.T., Kohnle U. (2016) Review on the projections of future storminess over the North Atlantic European region. *Atmosphere* **7**, 60, doi: 10.3390/atmos7040060.

Murphy M.J., Porcelli D., Pogge von Strandmann P.A.E., Hirst C.A., Kutscher L., Katchinoff J.A., Mörth C.-M., Maximov T., Andersson P.S. (2019) Tracing silicate weathering processes in the permafrost-dominated Lena River watershed using lithium isotopes. *Geochim. Cosmochim. Acta* **245**, 154-171.

Murphy P.J., Smallshire R., Midgley C. (2001) The sediments of Illusion Pot, Kingsdale, UK: Evidence for sub-glacial utilisation of a karst conduit in the Yorkshire Dales? *Cave and Karst Science* **28**, 29-34.

Négrel P., Millot R., Brenot A., Bertin C. (2010) Lithium isotopes as tracers of groundwater circulation in a peat land. *Chemical Geology* **276**, 119-127.

Négrel P., Millot R., Petelet-Giraud E., Klaver G. (2020) Li and δ^7Li as proxies for weathering and anthropogenic activities: Application to the Dommel River (Meuse Basin). *Appl. Geochem.* **120**, 104674.

Oelkers E.H., Butcher R., Pogge von Strandmann P.A.E., Schuessler J.A., Von Blanckenburg F., Snæbjörnsdóttir S.Ó., Mesfin K., Aradóttir E.S., Gunnarsson I., Sigfússon B., Gunnlaugsson E., Matter J.M., Stute M., Gislason S.R. (2019) Using stable Mg isotope signatures to assess the fate of magnesium during the *in situ* mineralisation of CO_2 and H_2S at the CarbFix site in SW-Iceland. *Geochim. Cosmochim. Acta* **245**, 542-555.

Parkhurst D.L., Appelo C. (1999) User's guide to PHREEQC (Version 2): A computer program for speciation, batch-reaction, one-dimensional transport, and inverse geochemical calculations. *Water-resources investigations report* **99**, 312.

Pistiner J.S., Henderson G.M. (2003) Lithium-isotope fractionation during continental weathering processes. *Earth Planet. Sci. Lett.* **214**, 327-339.

Pogge von Strandmann P.A.E., Elliott T., Marschall H.R., Coath C., Lai Y.-J., Jeffcoate A.B., Ionov D.A. (2011) Variations of Li and Mg isotope ratios in bulk chondrites and mantle xenoliths. *Geochim. Cosmochim. Acta* **75**, 5247-5268.

Pogge von Strandmann P.A.E., Opfergelt S., Lai Y.-J., Sigfússon B., Gislason S.R., Burton K.W. (2012) Lithium, magnesium and silicon isotope behaviour accompanying weathering in a basaltic soil and pore water profile in Iceland. *Earth Planet. Sci. Lett.* **339**, 11-23.

Pogge von Strandmann P.A.E., Jenkyns H.C., Woodfine R.G. (2013) Lithium isotope evidence for enhanced weathering during Oceanic Anoxic Event 2. *Nat. Geosci.* **6**, 668-672.

Pogge von Strandmann P.A.E., Porcelli D., James R.H., Van Calsteren P., Schaefer B., Cartwright I., Reynolds B.C., Burton K.W. (2014) Chemical weathering processes in the Great Artesian Basin: Evidence from lithium and silicon isotopes. *Earth Planet. Sci. Lett.* **406**, 24-36.

Pogge von Strandmann P.A.E., Henderson G.M. (2015) The Li isotope response to mountain uplift. *Geology* **43**, 67-70.

Pogge von Strandmann P.A.E., Burton K.W., Opfergelt S., Eiríksdóttir E.S., Murphy M.J., Einarsson A., Gislason S.R. (2016) The effect of hydrothermal spring weathering processes and primary productivity on lithium isotopes: Lake Myvatn, Iceland. *Chemical Geology* **445**, 4-13.

Pogge von Strandmann P.A.E., Frings P.J., Murphy M.J. (2017a) Lithium isotope behaviour during weathering in the Ganges Alluvial Plain. *Geochim. Cosmochim. Acta* **198**, 17-31.

Pogge von Strandmann P.A.E., Desrochers A., Murphy M.J., Finlay A.J., Selby D., Lenton T.M. (2017b) Global climate stabilisation by chemical weathering during the Hirnantian glaciation. *Geochemical Perspectives Letters* **3**, 230-237.

Pogge von Strandmann P.A.E., Vaks A., Bar-Matthews M., Ayalon A., Jacob E., Henderson G.M. (2017c) Lithium isotopes in speleothems: Temperature-controlled variation in silicate weathering during glacial cycles. *Earth Planet. Sci. Lett.* **469**, 64-74.

Pogge von Strandmann P.A.E., Fraser W.T., Hammond S.J., Tarbuck G., Wood I.G., Oelkers E.H., Murphy M.J. (2019) Experimental determination of Li isotope behaviour during basalt weathering. *Chemical Geology* **517**, 34-43.

Pokrovski G.S., Schott J., Salvi S., Gout R., Kubicki J.D. (1998) Structure and stability of aluminum-silica complexes in neutral to basic solutions. Experimental study and molecular orbital calculations. *Mineralogical Magazine A* **62**, 1194-1195.

Rau G.C., Cuthbert M.O., Andersen M.S., Baker A., Rutlidge H., Markowska M., Roshan H., Marjo C.E., Graham P.W., Acworth R.I. (2015) Controls on cave drip water temperature and implications for speleothem-based paleoclimate reconstructions. *Quat. Sci. Rev.* **127**, 19-36.

Roberts M.S., Smart P.L., Hawkesworth C.J., Perkins W.T., Pearce N.J.G. (1999) Trace element variations in coeval Holocene speleothems from GB Cave, southwest England. *The Holocene* **9**, 707-713.

Rose J. (1991) Drumlin sediments, Widdale Side, in: Mitchell W.A. (Ed.), *Western Pennines: Field Guide*. Quaternary Research Association, London, pp. 61-65.

Rudnick R.L., Gao S. (2003) Composition of the continental crust, in: Elderfield H. (Ed.), *The Oceans and Marine Geochemistry*. Elsevier-Pergamon, Oxford, pp. 1-64.

Ryu J.-S., Vigier N., Lee S.-W., Lee K.-S., Chadwick O.A. (2014) Variation of lithium isotope geochemistry during basalt weathering and secondary mineral transformations in Hawaii. *Geochim. Cosmochim. Acta* **145**, 103-115.

Samaniego L., Thober S., Kumar R., Wanders N., Rakovec O., Pan M., Zink M., Sheffield J., Wood E.F., Marx A. (2018) Anthropogenic warming exacerbates European soil moisture droughts. *Nat. Clim. Chang.* **8**, 421-426.

Stefánsson A., Gíslason S.R. (2001) Chemical weathering of basalts, Southwest Iceland: effect of rock crystallinity and secondary minerals on chemical fluxes to the ocean. *Am. J. Sci.* **301**, 513-556.

Steinhoefel G., Brantley S.L., Fantle M.S. (2021) Lithium isotopic fractionation during weathering and erosion of shale. *Geochim. Cosmochim. Acta* **295**, 155-177.

Teng F.-Z., McDonough W.F., Rudnick R.L., Dalpé C., Tomascak P.B., Chappell B.W., Gao S. (2004) Lithium isotopic composition and concentration of the upper continental crust. *Geochim. Cosmochim. Acta* **68**, 4167-4178.

Tessier A., Campbell P.G.C., Bisson M. (1979) Sequential extraction procedure for the speciation of particulate trace metals. *Anal. Chem.* **51**, 844-851.

Tipper E.T., Bickle M.J., Galy A., West A.J., Pomiès C., Chapman H.J. (2006) The short term climatic sensitivity of carbonate and silicate weathering fluxes: insight from seasonal variations in river chemistry. *Geochim. Cosmochim. Acta* **70**, 2737-2754.

Tipper E.T., Lemarchand E., Hindshaw R.S., Reynolds B.C., Bourdon B. (2012) Seasonal sensitivity of weathering processes: Hints from magnesium isotopes in a glacial stream. *Chemical Geology* **312**, 80-92.

Treble P.C., Bradley C., Wood A., Baker A., Jex C.N., Fairchild I.J., Gagan M.K., Cowley J., Azcurra C. (2013) An isotopic and modelling study of flow paths and storage in Quaternary calcarenite, SW Australia: implications for speleothem paleoclimate records. *Quat. Sci. Rev.* **64**, 90-103.

Vigier N., Decarreau A., Millot R., Carignan J., Petit S., France-Lanord C. (2008) Quantifying Li isotope fractionation during smectite formation and implications for the Li cycle. *Geochim. Cosmochim. Acta* **72**, 780-792.

Walker J.C.G., Hays P.B., Kasting J.F. (1981) A negative feedback mechanism for the long-term stabilization of earth's surface temperature. *Journal of Geophysical Research-Oceans and Atmospheres* **86**, 9776-9782.

Waltham A.C. (1970) Shale units in the Great Scar Limestone of the southern Askrigg Block. *Proceedings of the Yorkshire Geological Society* **38**, 285-292.

Waltham T., Lowe D. (2017) *Caves and Karst of the Yorkshire Dales, Volume 2 The Caves*. British Cave Research Association, Buxton.

Wanner C., Sonnenthal E.L., Liu X.-M. (2014) Seawater δ^7Li: A direct proxy for global CO_2 consumption by continental silicate weathering? *Chemical Geology* **381**, 154-167.

Wanner C., Bucher K., Pogge von Strandmann P.A.E., Waber H.N., Pettke T. (2017) On the use of Li isotopes as a proxy for water–rock interaction in fractured crystalline rocks: A case study from the Gotthard rail base tunnel. *Geochim. Cosmochim. Acta* **198**, 396-418.

Waters C., Lowe D. (2017) Chapter 2: Geology of the limestones, in: Waltham T., Lowe D. (Eds.), *Caves and Karst of the Yorkshire Dales, Volume 1*. British Cave Research Association, Buxton.

West A.J. (2012) Thickness of the chemical weathering zone and implications for erosional and climatic drivers of weathering and for carbon-cycle feedbacks. *Geology* **40**, 811-814.

Wimpenny J., Gíslason S.R., James R.H., Gannoun A., Pogge von Strandmann P.A.E., Burton K.W. (2010) The behaviour of Li and Mg isotopes during primary phase dissolution and secondary mineral formation in basalt. *Geochim. Cosmochim. Acta* **74**, 5259-5279.

Wimpenny J., Colla C.A., Yu P., Yin Q.-Z., Rustad J.R., Casey W.H. (2015) Lithium isotope fractionation during uptake by gibbsite. *Geochim. Cosmochim. Acta* **168**, 133-150.

Yeghicheyan D., Carignan J., Valladon M., Bouhnik Le Coz M., Le Cornec F., Castrec-Rouelle M., Robert M., Aquilina L., Aubry E., Churlaud C., Dia A., Deberdt S., Dupré B., Freydier R., Gruau G., Hénin O., De Kersabiec A.-M., Macé J., Marin L., Morin N., Petitjean P., Serrat E. (2001) A compilation of silicon and thirty one trace elements measured in the natural river water reference material SLRS-4 (NRC-CNRC). *Geostandards Newsletter* **25**, 465-474.

Zhang X., Saldi G.D., Schott J., Bouchez J., Kuessner M., Montouillout V., Henehan M., Gaillardet J. (2021) Experimental constraints on Li isotope fractionation during the interaction between kaolinite and seawater. *Geochim. Cosmochim. Acta* **292**, 333-347.

Figures

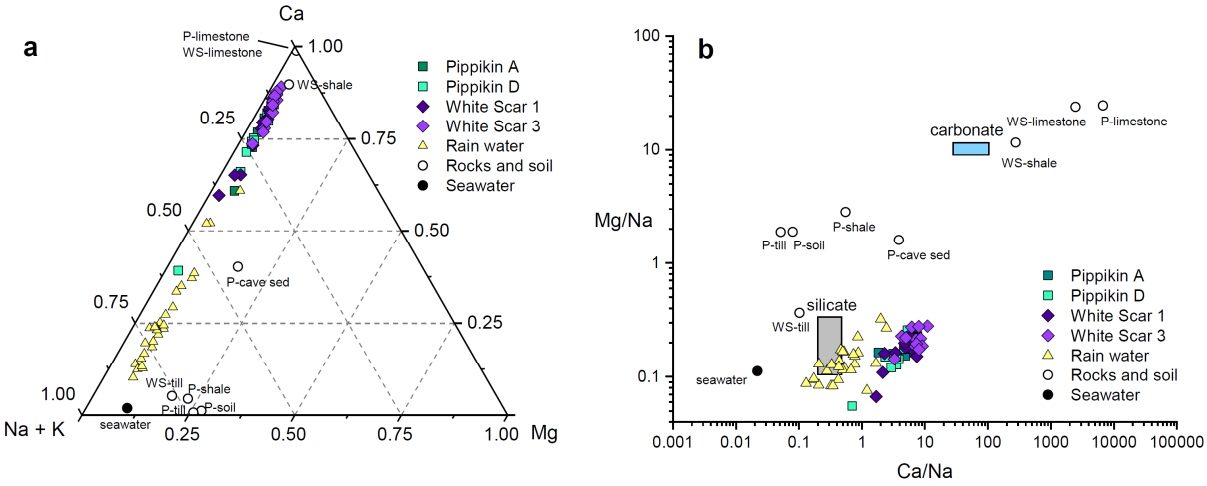

Fig. 1: Major element chemistry of the cave drip-waters and rain waters, compared to local lithogenic sources and seawater. (a) Ternary plot of Ca-Mg-(Na+K) molar proportions. (b) Molar ratios of Mg/Na versus Ca/Na. See Table 2 for full sample details of the local rocks and soils. Prefixes 'P' and 'WS' indicate samples from the vicinity of Pippikin cave and White Scar Cave, respectively. Note that the representative global silicate and carbonate endmembers in panel (b) indicate typical values based on river chemistry (Gaillardet et al., 1999) rather than the full range of potential variation in source rocks.

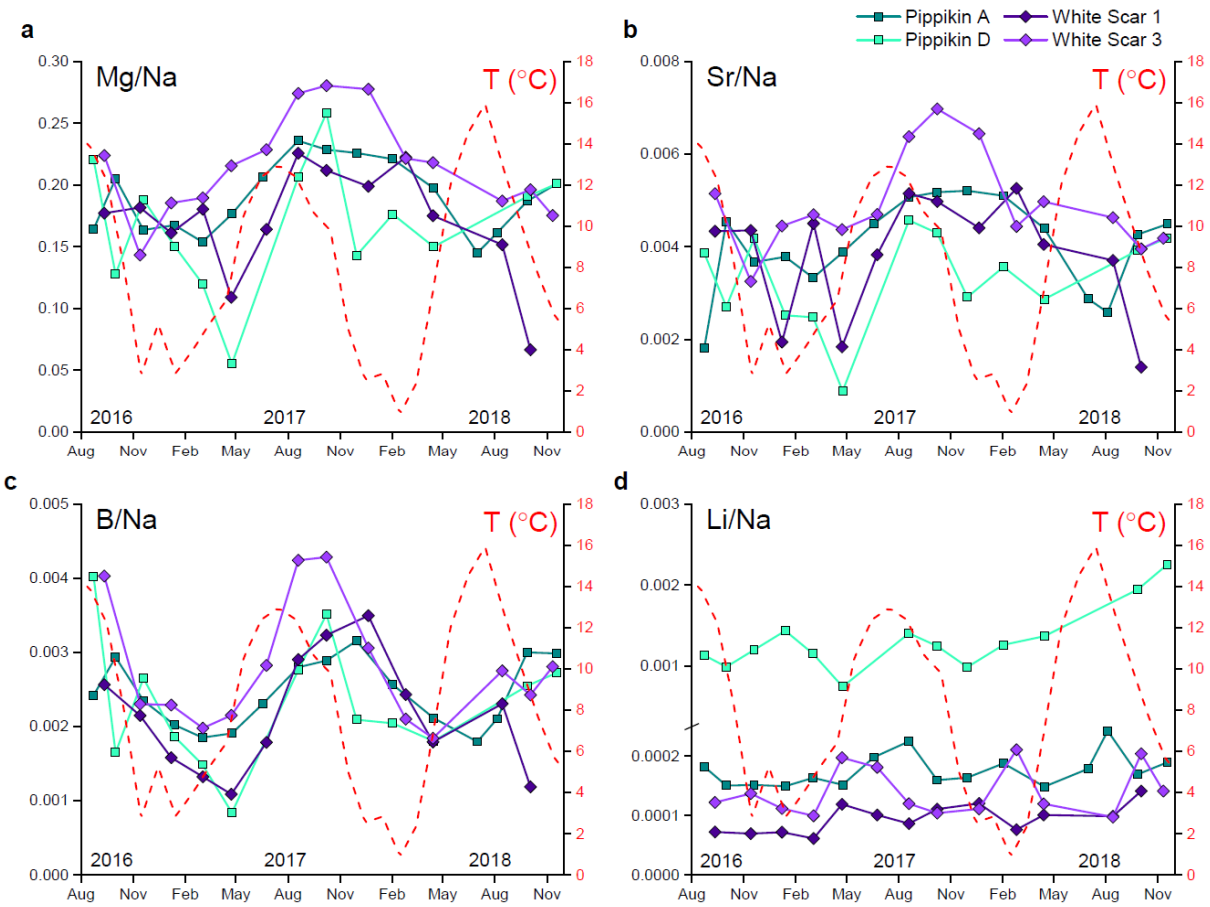

Fig. 2: Time series of drip-water chemistry plotted as molar ratios: (a) Mg/Na, (b) Sr/Na, (c) B/Na, (d) Li/Na. Red dashed line indicates monthly surface air temperatures outside Pippikin cave.

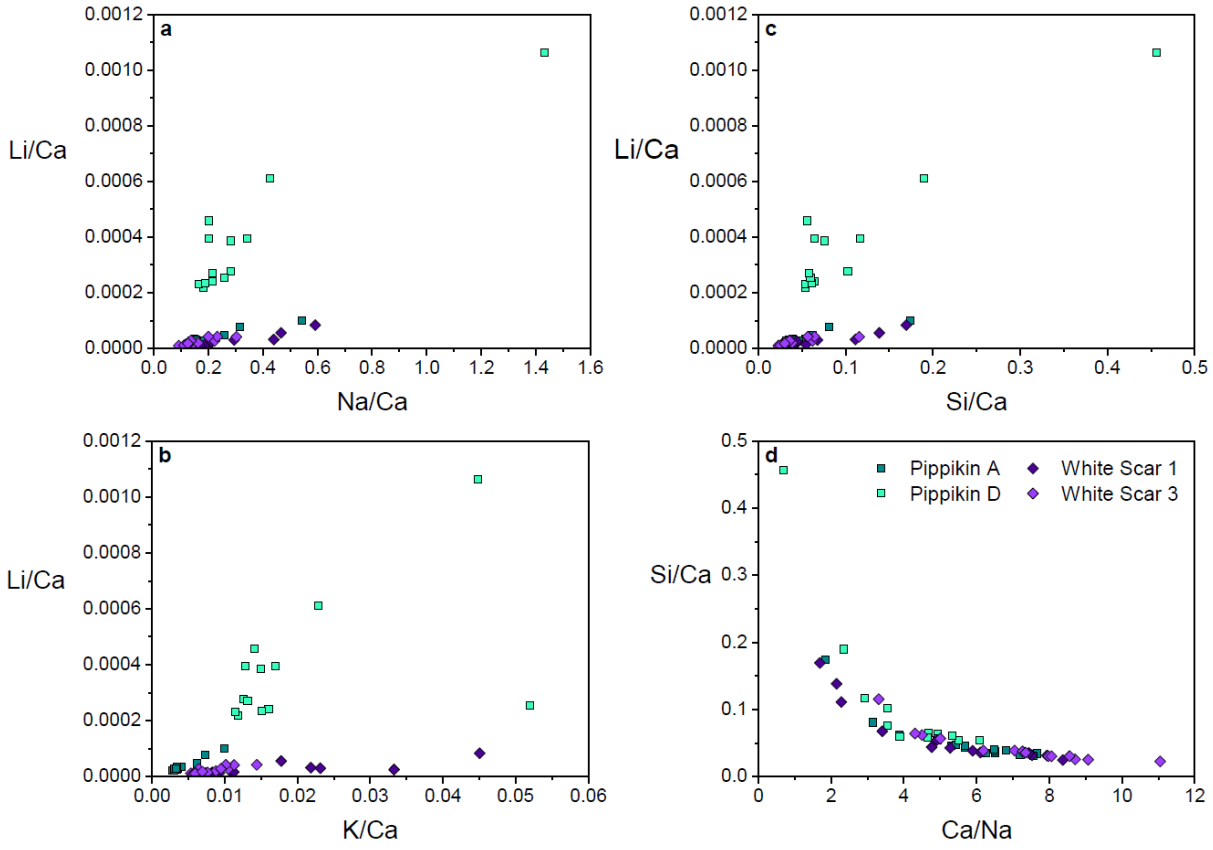

Fig. 3: Cross plots of drip-water Li/Ca molar ratios against (a) Na/Ca, (b) K/Ca, and (c) Si/Ca, and (d) cross plot of Si/Ca against Ca/Na, indicating mixing between silicate and carbonate endmembers.

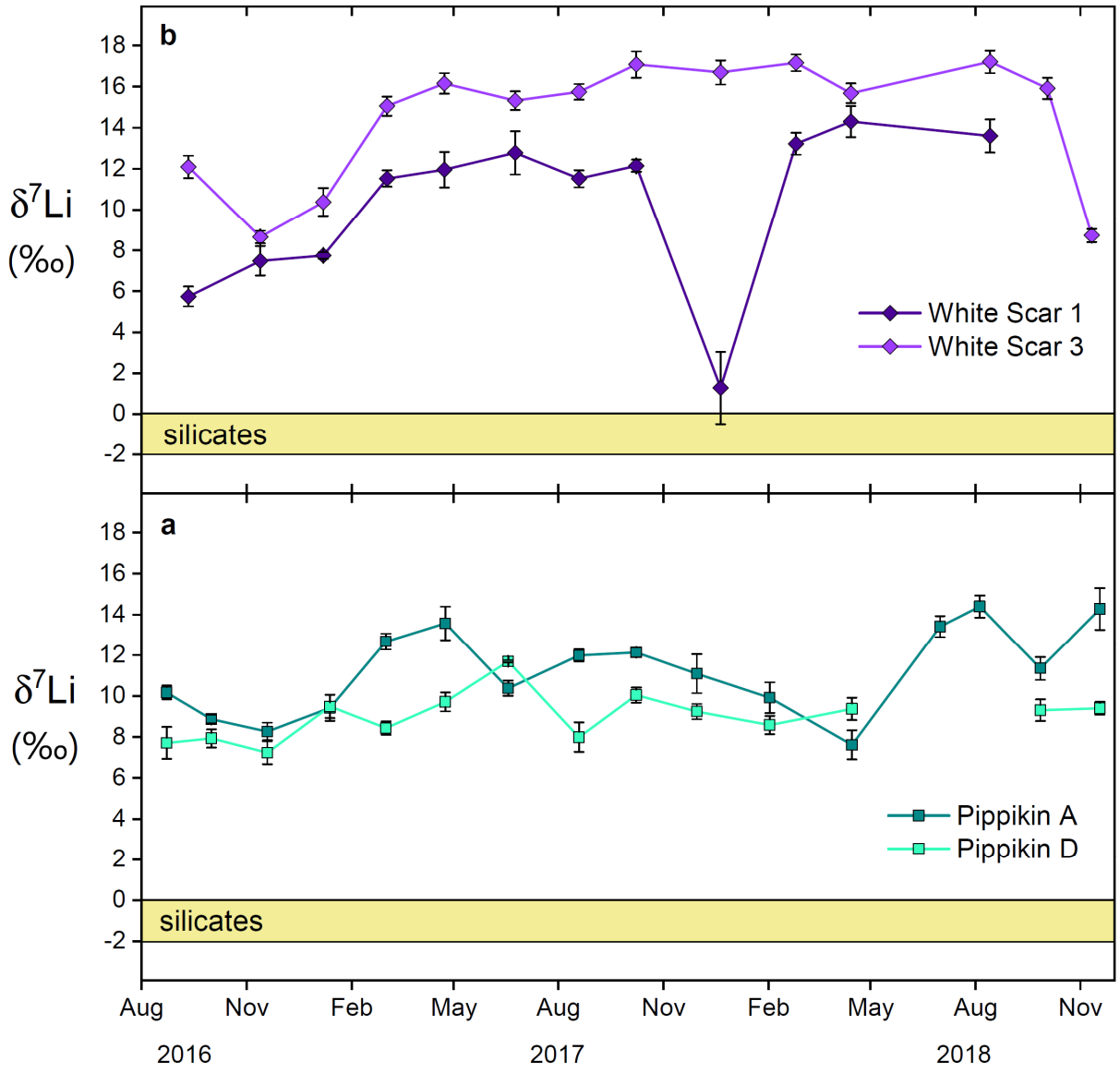

Fig. 4: Time series of drip-water Li isotopes for (a) Pippikin cave, and (b) White Scar Cave. Yellow bar indicates the Li isotope composition of local silicate sources (see Fig. 5a). Error bars for drip-water data represent 2sd (see Table 1).

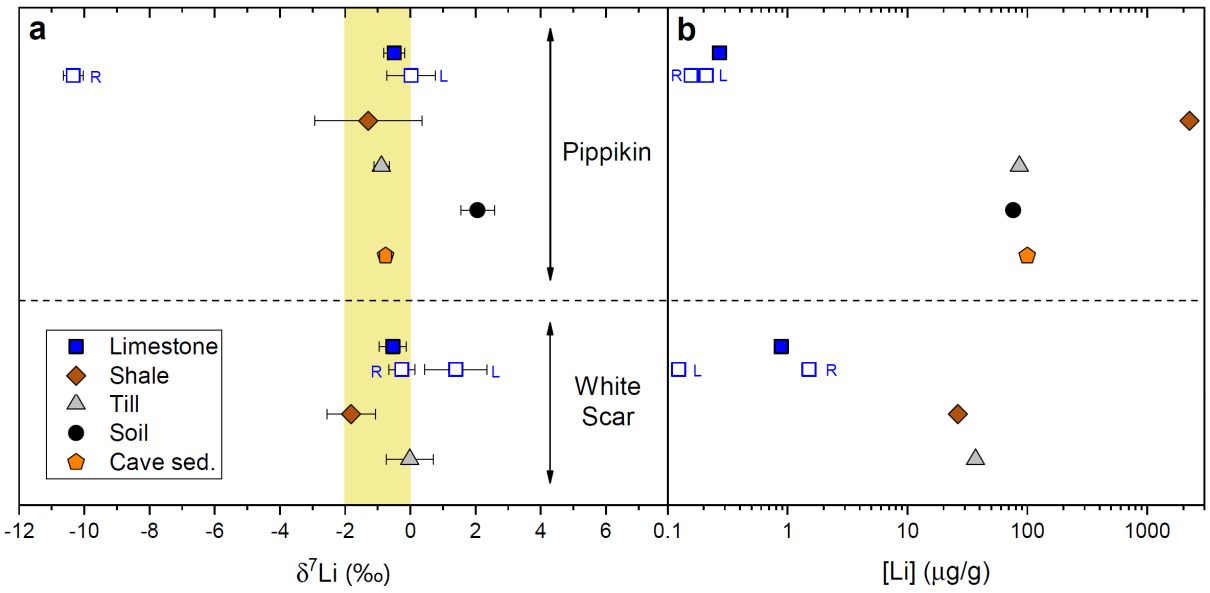

Fig. 5: Composition of local rocks, sediments, tills, and soils at Pippikin cave and White Scar Cave (see Table 2 and text for sample details): (a) Li isotopes, (b) Li concentrations (on a logarithmic scale). Open blue squares represent leachates (L) and residues (R) of the limestone. In panel (a), the yellow bar highlights the Li isotope range of all bulk samples (excluding the peaty soil). Error bars for Li isotopes represent 2sd.

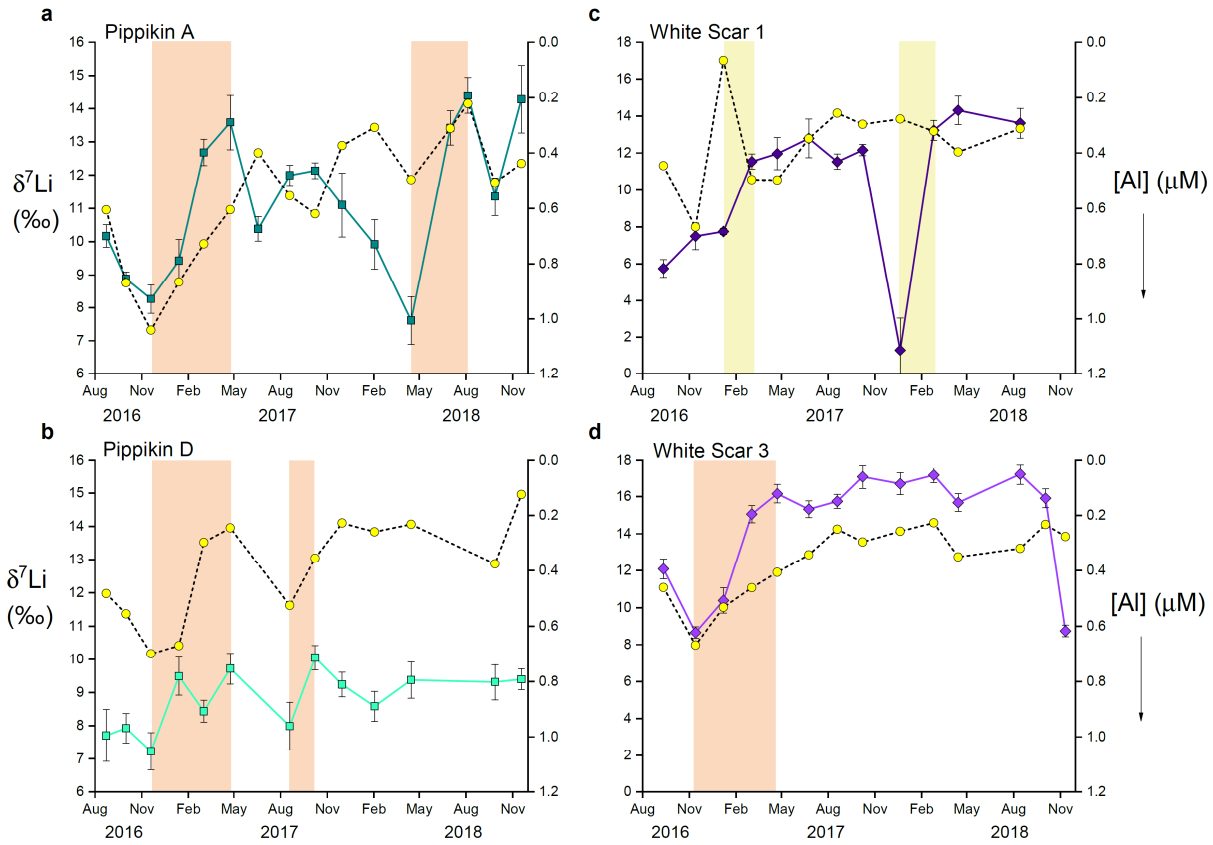

Fig. 6: Temporal variability in Li isotopes (coloured symbols and solid lines) and Al concentrations (yellow circles and dashed black lines) at each of the four sites: (a) Pippikin A; (b) Pippikin D; (c) White Scar 1; (d) White Scar 3. Note that the Li isotope data are on separate y-axes for Pippikin cave and White Scar Cave, whereas the Al data are on the same (reversed) y-axis for all sites. Orange bars indicate the main intervals when Li isotopes shifted towards higher values accompanied by decreasing Al concentrations, while yellow bars indicate shifts towards higher Li isotope values at White Scar 1 that were not accompanied by obvious changes in Al concentrations.

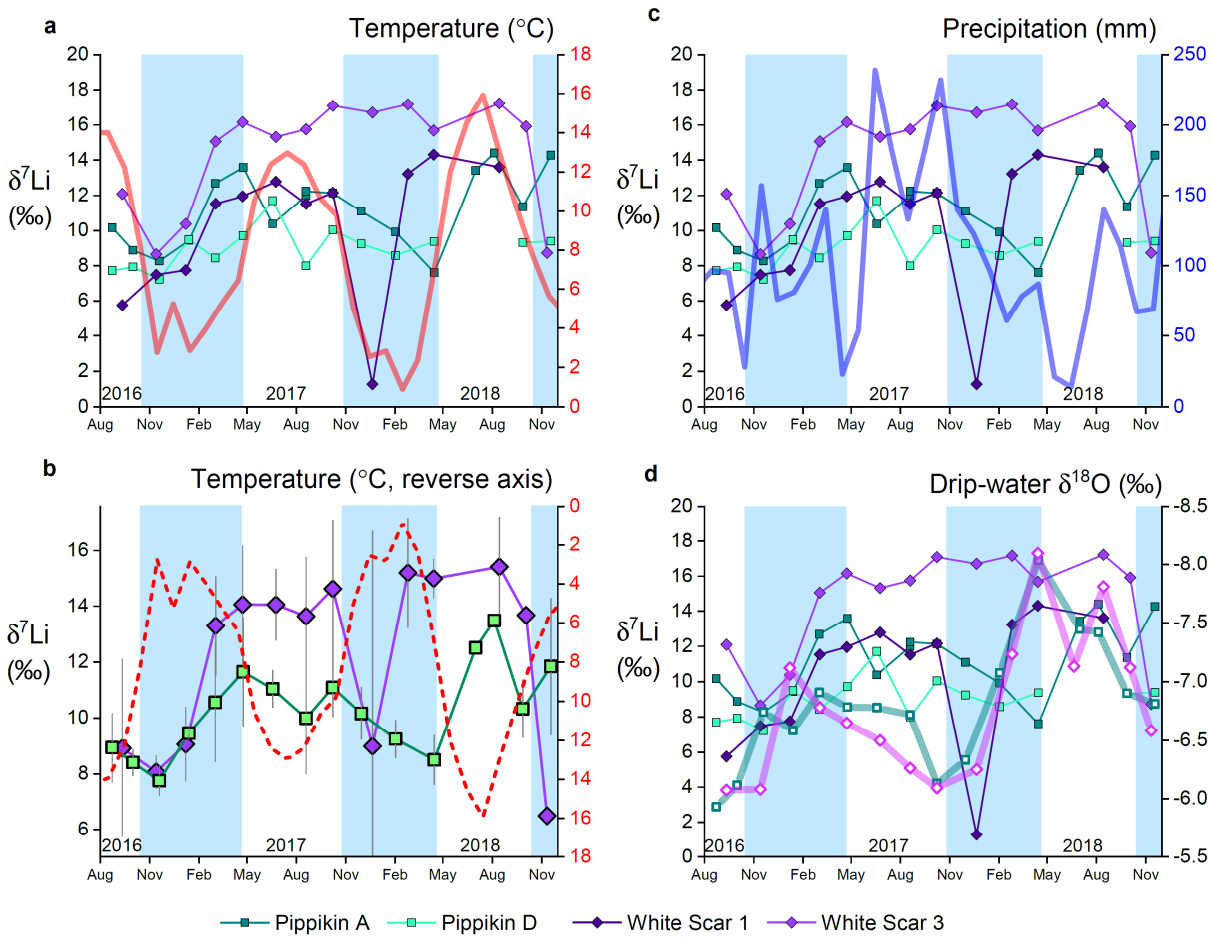

Fig. 7: Time series of drip-water δ^7Li values (symbols and lines) compared to (a) monthly surface air temperature outside Pippikin cave (red line); (b) temperature as in panel (a) but on a reverse axis (red dashed line); (c) monthly precipitation (blue line); and (d) drip-water δ^{18}O (thick green line, Pippikin cave; thick purple line, White Scar Cave; plotted values are the mean of the two drip sites for each cave; note inverted axis). In panel (b), the δ^7Li values are the mean of the two drip sites in each cave (green symbols and line, Pippikin cave; purple symbols and line, White Scar Cave), with the vertical bars indicating the range of measured values rather than representing error bars. Note that where δ^7Li data exist for only one of the two sites in a given cave, the measured value is adjusted by half the mean δ^7Li offset between the two sites to account for inter-site variability. In all panels, blue bars highlight cold intervals with below average monthly air temperatures.

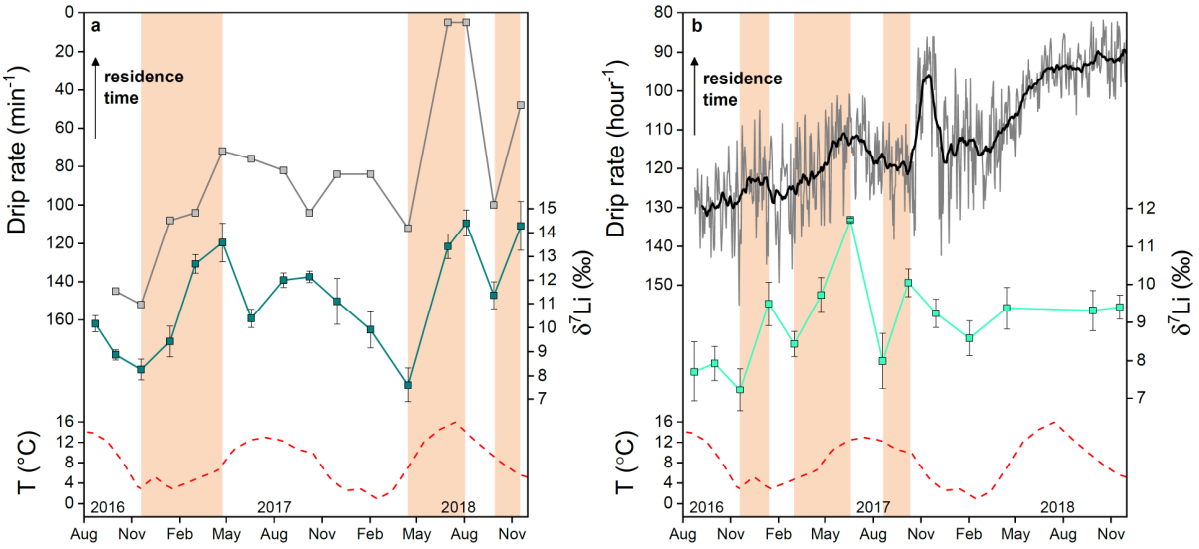

Fig. 8: Time series from (a) Pippikin A and (b) Pippikin D of drip rates (note inverted axes), drip-water Li isotopes, and monthly surface air temperatures (measured outside Pippikin cave). Drip rates in (a) are from instantaneous measurements during drip-water sampling. Drip rates in (b) are from the nearby "Stalagmate" drip logger rather than the drip site itself (grey line, daily drip rates; black line, monthly-smoothed). Note the differing units for drip rates between panels (a) and (b). Orange bars indicate intervals when Li isotopes shifted towards higher values, which were generally accompanied by lower drip rates that are inferred to reflect longer fluid residence times (indicated by arrows).

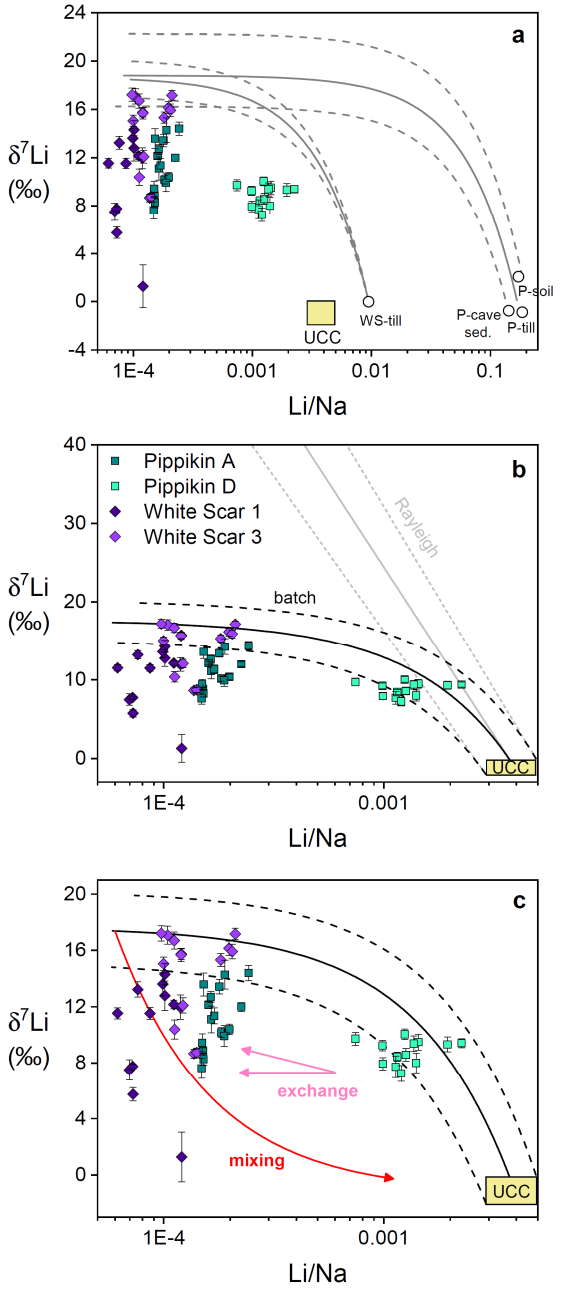

Fig. 9: Cross plots of drip-water δ^7Li values against Li/Na molar ratios, compared to modelled fluid evolution during secondary clay removal. (a) Batch (equilibrium) fractionation curves from an initial fluid with the composition of local till at White Scar Cave, or with the mean composition of local till, soil, and cave sediment at Pippikin cave (see Table 2 for sample details; prefixes 'P' and 'WS' indicate Pippikin and White Scar, respectively). (b) Batch (equilibrium) fractionation curve (black) and Rayleigh fractionation curve (grey) based on an initial fluid derived from a silicate source with δ^7Li = -1 ± 1 ‰ (Fig. 5a) and Li/Na ratio of the upper continental crust (UCC) (0.0029-0.0049) (Rudnick and Gao, 2003; Teng et al., 2004). (c) Multi-step evolution including batch fractionation as in (b) followed by either mixing with a silicate-derived fluid source or adsorption/exchange with secondary clay minerals. For all panels, the fractionation factor $\alpha_{clay\text{-}fluid}$ is 0.9815 (range of 0.983-0.980), based on temperature-adjusted experimental data for clays (Li and West, 2014; Gou et al., 2019; Hindshaw et al., 2019a). Solid lines indicate the most likely fluid evolution, while dashed lines indicate upper and lower bounds based on those parameter ranges. In panel (c), the "mixing" arrow models a starting point on the batch fractionation curve at Li/Na = 0.00006 (i.e. matching the lowest recorded drip-water Li/Na value) followed by mixing with a silicate-derived fluid source (δ^7Li = -1 ‰ and Li/Na = 0.0039), while the "exchange" arrows schematically indicate adsorption/exchange with clay minerals involving a smaller magnitude of fractionation or no fractionation (see text). Note logarithmic x-axes for all panels and the different x-axis scale for panel (a).

Tables

Table 1: Analyses of cave drip-waters for drip rates, oxygen isotopes, major and trace elements, and Li isotopes

Location	Date	Drip rate min^{-1}	$\delta^{18}O$ ‰	Ca µmol/L	Mg µmol/L	Na µmol/L	K µmol/L	Si µmol/L	Sr nmol/L	B nmol/L	Al nmol/L	Ti nmol/L	Mo nmol/L	Ba nmol/L	U nmol/L	Li nmol/L	Li/Na molar	$\delta^{7}Li$ ‰	2sd ‰
Pip A	23-Aug-16	-	-6.33	487	43.5	265	4.9	84.7	483	640	610	4.6	3.4	48.2	1.4	48	0.00018	10.2	0.3
Pip A	01-Oct-16	145	-5.86	1140	44.0	214	4.0	51.7	973	630	870	6.7	2.2	172	2.3	32	0.00015	8.9	0.2
Pip A	19-Nov-16	152	-6.40	1140	34.4	211	3.8	53.3	773	500	1040	6.2	3.5	86.5	2.6	32	0.00015	8.3	0.4
Pip A	13-Jan-17	108	-7.21	1100	32.4	193	3.7	48.0	731	390	870	7.5	3.8	78.5	2.5	29	0.00015	9.4	0.6
Pip A	03-Mar-17	104	-6.98	1010	31.7	206	4.0	54.6	685	380	730	7.8	3.7	81.7	2.3	34	0.00016	12.7	0.4
Pip A	24-Apr-17	72	-6.65	1010	31.3	177	3.5	46.5	688	340	600	5.3	3.6	76.6	2.2	27	0.00015	13.6	0.8
Pip A	18-Jun-17	76	-6.73	1220	38.8	188	4.2	42.8	845	430	400	3.4	3.0	136	2.0	37	0.00020	10.4	0.4
Pip A	19-Aug-17	82	-6.62	1350	46.6	198	4.7	53.0	1000	550	550	3.2	2.6	180	2.3	44	0.00023	12.0	0.3
Pip A	19-Aug-17	replicate[a]	-	-	-	-	-	-	-	-	-	-	-	-	-	-	-	12.2	0.6
Pip A	08-Oct-17	104	-6.26	1410	42.1	184	3.9	48.4	952	530	620	3.9	2.7	111	2.6	29	0.00016	12.1	0.2
Pip A	30-Nov-17	84	-5.94	1140	34.0	151	3.1	34.9	784	480	370	3.5	2.3	83.5	2.2	25	0.00016	11.1	1.0
Pip A	02-Feb-18	84	-7.17	1070	32.8	149	3.4	34.5	757	380	310	3.2	3.0	454	2.2	28	0.00019	9.9	0.7
Pip A	15-Apr-18	112	-8.47	1060	32.0	162	3.3	39.2	714	340	500	3.6	3.0	121	2.0	24	0.00015	7.6	0.7
Pip A	01-Jul-18	<5	-7.45	963	36.1	249	6.0	60.1	717	450	310	3.1	3.5	106	1.7	45	0.00018	13.4	0.5
Pip A	05-Aug-18	<5	-7.51	760	38.8	241	5.6	61.2	622	510	220	4.6	4.1	147	1.6	59	0.00024	14.4	0.5
Pip A	27-Sep-18	100	-6.59	1060	31.6	169	3.2	37.3	723	510	510	2.8	2.8	95.6	1.9	29	0.00017	11.4	0.6
Pip A	18-Nov-18	48	-6.36	1020	31.7	158	3.4	41.4	707	470	440	4.6	3.2	152	2.1	30	0.00019	14.3	1.0
Pip D	23-Aug-16	64	-5.53	827	39.0	177	13.3	53.4	682	710	480	8.0	2.8	83.3	1.4	200	0.00113	7.7	0.8
Pip D	01-Oct-16	10	-6.37	1450	52.2	408	18.3	149	1110	670	560	11.6	6.5	197	2.9	403	0.00099	7.9	0.4
Pip D	19-Nov-16	68	-7.08	1060	36.3	193	12.6	57.3	807	510	700	6.9	3.9	161	1.8	231	0.00120	7.2	0.6
Pip D	13-Jan-17	9	-5.96	863	55.4	368	19.8	164	927	690	670	12.3	8.7	126	2.8	527	0.00143	9.5	0.6
Pip D	03-Mar-17	8	-6.84	1110	45.5	379	18.8	129	938	560	300	11.0	9.1	162	2.6	435	0.00115	8.4	0.3
Pip D	24-Apr-17	6	-6.92	774	61.3	1110	34.7	353	984	930	250	20.8	13.3	111	2.9	823	0.00074	9.7	0.5
Pip D	18-Jun-17	6	-6.83	-	-	-	-	-	-	-	-	-	-	-	-	-	-	11.7	0.1
Pip D	19-Aug-17	12	-6.82	1540	52.3	254	17.7	82.8	1160	700	530	8.5	5.2	190	2.9	356	0.00140	8.0	0.7
Pip D	08-Oct-17	48	-6.00	961	46.5	180	14.5	58.8	774	630	355	4.7	3.2	141	1.7	224	0.00125	10.1	0.4
Pip D	30-Nov-17	8	-6.73	1370	50.3	352	71.2	81.6	1030	740	230	10.8	7.9	240	2.8	347	0.00099	9.2	0.4
Pip D	02-Feb-18	10	-6.98	1340	50.8	288	17.7	78.2	1030	590	260	13.3	7.9	157	3.1	363	0.00126	8.6	0.5
Pip D	15-Apr-18	6	-7.60	1350	57.0	380	20.2	102	1090	690	230	14.4	9.6	174	3.2	520	0.00137	9.4	0.5
Pip D	01-Jul-18	no drip	-	-	-	-	-	-	-	-	-	-	-	-	-	-	-	-	-
Pip D	05-Aug-18	-	-7.33	-	-	-	-	-	-	-	-	-	-	-	-	-	-	-	-
Pip D	27-Sep-18	7	-7.21	1620	62.7	329	20.9	103	1290	840	380	16.2	8.7	243	3.8	639	0.00194	9.3	0.5
Pip D	18-Nov-18	6	-7.27	1630	66.4	330	23.0	91.4	1390	900	130	17.6	9.5	263	4.3	745	0.00225	9.4	0.3
WS 1	11-Sep-16	-	-6.22	1560	45.4	256	12.8	56.2	1110	660	450	2.8	1.0	46.2	1.2	19	0.00007	5.7	0.5
WS 1	13-Nov-16	-	-6.08	1070	39.7	218	11.7	58.1	949	470	670	3.2	0.9	36.6	1.2	15	0.00007	7.5	0.7
WS 1	07-Jan-17	continuous	-7.01	488	34.5	214	10.6	54.2	417	340	70	3.0	0.8	15.8	0.6	15	0.00007	7.7	0.2
WS 1	04-Mar-17	continuous	-6.84	1670	35.9	199	11.4	41.0	896	260	500	3.2	0.7	38.1	1.3	12	0.00006	11.5	0.4
WS 1	23-Apr-17	70	-6.64	666	33.9	310	11.8	92.2	571	340	500	3.7	1.5	30.0	1.3	37	0.00012	12.0	0.9
WS 1	24-Jun-17	54	-6.57	864	41.6	254	20.0	58.4	971	450	350	3.0	1.1	46.0	1.1	26	0.00010	12.8	1.0
WS 1	19-Aug-17	continuous	-6.24	1230	52.5	233	13.8	52.6	1200	680	260	2.6	0.7	51.4	1.2	20	0.00009	11.5	0.4
WS 1	08-Oct-17	continuous	-6.09	1780	50.1	236	14.8	57.1	1180	760	300	3.5	1.8	60.6	1.4	26	0.00011	12.2	0.3
WS 1	21-Dec-17	212	-6.23	1060	44.1	222	35.1	46.3	977	780	280	3.4	45.2	128	1.3	27	0.00012	1.3	1.8

WS 1	25-Feb-18	-	-7.11	1020	38.6	173	9.4	39.2	912	420	320	3.0	1.2	34.8	1.5	13	0.00008	13.2	0.5
WS 1	14-Apr-18	continuous	-8.26	1750	38.7	221	12.9	54.8	894	400	400	4.0	1.2	57.2	1.3	22	0.00010	14.3	0.8
WS 1	20-Jun-18	98	-7.05	-	-	-	-	-	-	-	-	-	-	-	-	-	-	-	-
WS 1	14-Aug-18	-	-7.81	1640	33.4	220	13.7	57.2	815	510	310	4.9	1.0	43.6	1.1	22	0.00010	13.6	0.8
WS 1	03-Oct-18	34	-7.03	923	36.4	545	41.6	156	766	650	330	3.7	2.5	150	1.2	77	0.00014	-	-
WS 1	11-Nov-18	84	-6.63	-	-	-	-	-	-	-	-	-	-	-	-	-	-	-	-
WS 3	11-Sep-16	-	-5.93	1010	50.2	224	10.6	62.6	1150	900	460	3.0	1.3	67.2	1.0	27	0.00012	12.1	0.5
WS 3	13-Nov-16	-	-6.08	924	40.0	279	10.4	107	908	640	670	5.1	2.1	46.0	1.3	38	0.00014	8.7	0.3
WS 3	07-Jan-17	continuous	-7.22	1450	38.1	205	9.3	56.1	912	470	530	4.1	1.5	51.0	1.1	23	0.00011	10.4	0.7
WS 3	04-Mar-17	continuous	-6.72	1660	36.2	191	8.9	42.9	895	380	460	4.1	1.0	37.5	1.1	19	0.00010	15.1	0.5
WS 3	23-Apr-17	130	-6.66	1550	46.1	214	9.9	58.6	936	460	410	4.7	1.6	125	1.4	42	0.00020	16.2	0.5
WS 3	24-Jun-17	93	-6.43	941	50.0	219	13.6	60.3	1030	620	340	3.0	1.4	172	1.2	40	0.00018	15.3	0.5
WS 3	19-Aug-17	continuous	-6.29	1270	56.3	206	11.2	49.2	1310	870	250	3.1	1.0	60.1	1.2	25	0.00012	15.7	0.4
WS 3	08-Oct-17	continuous	-	2030	51.4	184	11.5	45.9	1280	790	300	3.2	1.6	57.9	1.2	19	0.00010	17.1	0.6
WS 3	21-Dec-17	continuous	-6.27	1270	44.0	159	9.7	38.7	1020	490	260	3.8	1.1	43.9	1.1	18	0.00011	16.7	0.6
WS 3	25-Feb-18	-	-7.36	1010	44.8	202	10.3	57.2	898	430	230	5.5	1.8	77.6	1.4	43	0.00021	17.2	0.4
WS 3	14-Apr-18	continuous	-7.92	1620	41.4	190	9.6	49.6	943	350	350	5.6	2.0	58.6	1.3	23	0.00012	15.7	0.5
WS 3	20-Jun-18	130	-7.21	-	-	-	-	-	-	-	-	-	-	-	-	-	-	-	-
WS 3	14-Aug-18	-	-7.81	1590	32.8	175	9.4	39.9	812	480	320	5.4	1.3	48.4	1.0	17	0.00010	17.2	0.5
WS 3	03-Oct-18	46	-7.21	1540	41.1	209	14.6	55.0	828	510	230	4.5	1.8	166	1.3	43	0.00020	15.9	0.5
WS 3	11-Nov-18	continuous	-6.54	1460	31.7	181	10.1	44.0	758	510	280	3.9	1.6	197	1.0	26	0.00014	8.7	0.3

(-) : not determined.

[a] : full Li isotope replicate, including filtration, elemental separation, and mass spectrometry.

Lithium isotope standards yield $\delta^7Li = +31.3 \pm 0.6$ (2sd, n=24) for seawater and $\delta^7Li = +2.5 \pm 0.3$ (n=5) for BCR-2.

Table 2: Characterisation of local rocks, tills, and soil for Li isotopes, Li concentrations, and selected elemental ratios

Cave	Sample	δ^7Li ‰	2sd ‰	[Li] µg/g	Li/Na mol/mol	Al/Ca mmol/mol
Pippikin	Great Scar Limestone - bulk	-0.5	0.3	*0.27*	0.02	0.58
Pippikin	Great Scar Limestone - carbonate leach	0.0	0.7	*0.21*	0.02	0.24
Pippikin	Great Scar Limestone - residue	-10.3	0.3	*0.16*	0.02	0.78
Pippikin	interbedded shale, Arson Shaft, Ease Gill - bulk	-1.3	1.6	2260	3.40	141000
Pippikin	interbedded shale, Arson Shaft, Ease Gill - exchangeable	16.7	1.2	*0.79*	-	-
Pippikin	Quaternary till, Ease Gill - bulk	-0.9	0.2	86	0.19	619000
Pippikin	Quaternary till, Ease Gill - exchangeable	5.3	0.7	*0.03*	-	-
Pippikin	peaty soil, overlying Pippikin cave - bulk	2.1	0.5	76	0.17	447000
Pippikin	peaty soil, overlying Pippikin cave - exchangeable	16.7	0.3	*0.08*	-	-
Pippikin	cave sediment, floor of Pippikin cave - bulk	-0.8	0.2	100	0.14	5650
Pippikin	cave sediment, floor of Pippikin cave - exchangeable	-5.0	0.7	*0.10*	-	-
White Scar	Great Scar Limestone - bulk	-0.5	0.4	*0.89*	0.03	2.58
White Scar	Great Scar Limestone - carbonate leach	1.4	1.0	*0.12*	0.01	0.24
White Scar	Great Scar Limestone - residue	-0.3	0.4	*1.51*	0.10	10.5
White Scar	Yoredale Shale - bulk	-1.8	0.7	26	0.22	244
White Scar	Quaternary till - bulk	0.0	0.7	37	0.01	32400

For all the limestone data and all exchangeable fractions, Li concentrations are estimates based on the signal intensity from MC-ICP-MS (shown in italics).
All other elemental data are from ICP-OES (see Table EA3 for full elemental analyses).
(-): not determined.

Table EA1: Lithium isotope measurements of standards

Table EA1a: Seawater standards

Standard	δ^7Li	2sd	Li in splits
	‰	‰	%
Seawater	31.3	0.2	0.2
Seawater	31.4	0.6	0.1
Seawater	31.1	0.3	0.0
Seawater	31.0	0.3	0.0
Seawater	30.9	0.4	0.1
Seawater	32.2	0.1	0.1
Seawater	31.3	0.5	0.0
Seawater	31.4	0.4	0.0
Seawater	31.4	0.8	0.1
Seawater	31.4	0.5	0.1
Seawater	31.5	0.6	0.2
Seawater	31.5	0.6	0.1
Seawater	31.2	0.5	-
Seawater	31.5	0.4	0.4
Seawater	31.6	0.3	0.2
Seawater	31.3	0.1	0.7
Seawater	31.3	0.4	0.2
Seawater	31.5	0.3	0.2
Seawater	31.2	0.4	0.6
Seawater	30.8	0.2	0.1
Seawater	31.2	0.5	0.1
Seawater	31.8	0.2	0.1
Seawater	31.4	0.6	0.0
Seawater	31.5	0.6	0.0
Seawater	31.3	0.6	0.0
Seawater	31.1	0.5	0.1
Seawater	31.4	0.8	0.0
Seawater	31.0	0.4	0.1
Seawater mean, 2sd	**31.3**	**0.6**	

(-): not determined.

Table EA1b: Seawater standards with variable column yields

Standard	δ^7Li	2sd	Li in splits	δ^7Li offset	δ^7Li offset / % Li in splits
	‰	‰	%	‰	
Seawater - variable yield	32.1	0.5	0.4	0.8	2.0
Seawater - variable yield	35.6	0.7	2.3	4.3	1.9
Seawater - variable yield	42.4	0.8	8.2	11.1	1.4
Mean δ^7Li offset (‰) / % Li in splits					**1.7**

Table EA1c: BCR2 standards

Standard	δ^7Li	2sd
	‰	‰
BCR2	2.6	0.1
BCR2	2.7	0.2
BCR2	2.4	0.3
BCR2	2.5	0.1
BCR2	2.5	0.4
BCR2 mean, 2sd	**2.5**	**0.3**

Table EA2: Rain water trace element concentrations and Li isotopes

Date	Ca µmol/L	Mg µmol/L	Na µmol/L	K µmol/L	Si µmol/L	Sr nmol/L	B nmol/L	Al nmol/L	Ti nmol/L	Mo nmol/L	Ba nmol/L	Li nmol/L	Li/Na mol/mol	δ^7Li ‰	2sd[a] ‰	2sd[b] ‰	Yield[c]
Sep-16	37	15.1	133	82.9	10.2	37	400	125	8.2	3.4	16.9	20	0.00015	12.5	1.1	1.1	
Oct-16	125	21.0	162	48.9	12.5	97	550	157	8.3	3.5	19.0	30	0.00019	13.1	0.8	0.8	
Nov-16	19	4.4	36	5.5	9.6	17	30	93.0	3.0	1.0	6.5	12	0.00032	11.4	0.5	0.5	
Dec-16	29	16.1	172	18.5	8.1	33	150	64.0	4.2	1.2	8.5	33	0.00019	11.2	0.7	0.7	
Jan-17	19	12.5	143	7.2	1.7	28	150	17.1	2.2	1.0	5.5	23	0.00016	13.4	0.3	0.3	
Feb-17	17	6.9	81	4.5	11.9	20	bdl	123	2.8	0.7	14.7	22	0.00027	9.2	0.3	0.6	*
Mar-17	22	5.7	68	16.3	1.2	19	60	18.7	2.3	0.5	5.4	18	0.00026	-	-	-	
Apr-17	79	15.5	102	16.7	3.5	62	150	113	4.9	1.0	44.9	27	0.00027	9.4	0.8	0.8	
May-17	81	6.4	49	19.7	8.5	47	180	96.8	2.6	2.4	12.5	19	0.00040	12.2	0.9	0.9	
Jun-17	23	5.4	47	17.1	2.5	14	80	52.3	2.5	0.7	4.9	15	0.00032	13.9	0.3	0.4	*
Jul-17	32	12.2	70	78.9	12.1	19	820	139	5.9	5.6	4.0	19	0.00027	11.1	0.1	0.1	
Aug-17	28	8.9	64	26.4	11.2	17	370	102	5.5	2.1	8.7	15	0.00024	12.7	1.2	1.2	
Sep-17	40	12.8	77	41.5	5.2	29	270	87.6	4.3	1.0	12.7	33	0.00043	12.7	0.4	0.5	*
Oct-17	35	21.6	166	49.7	3.4	34	370	39.7	3.4	1.4	11.9	24	0.00015	-	-	-	
Nov-17	33	12.7	98	31.7	5.0	22	190	145	5.0	2.1	8.2	23	0.00024	-	-	-	
Dec-17	69	19.8	161	33.7	13.4	48	270	84.5	7.5	0.6	31.3	35	0.00022	-	-	-	
Jan-18	34	19.4	200	5.1	4.9	40	140	104	4.0	0.9	12.6	32	0.00016	-	-	-	
Feb-18	50	11.2	119	4.2	15.1	42	40	47.0	2.7	0.7	30.2	23	0.00019	-	-	-	
Mar-18	55	13.1	158	4.7	4.8	51	bdl	65.0	2.4	0.9	15.6	22	0.00014	-	-	-	
Apr-18	77	4.9	64	2.3	8.0	49	bdl	53.7	1.9	0.8	19.1	15	0.00023	-	-	-	
May-18	235	25.9	96	29.1	11.9	211	330	129	5.1	1.1	111	52	0.00054	-	-	-	
Jun-18	104	19.4	119	28.3	7.8	74	300	91.6	3.0	1.2	47.6	85	0.00072	-	-	-	
Jul-18	71	18.6	82	135	2.8	47	650	268	4.5	0.9	21.5	22	0.00027	-	-	-	
Aug-18	145	23.4	72	191	5.8	77	1420	449	11.1	0.8	20.7	23	0.00032	-	-	-	
Sep-18	95	16.3	141	149	6.3	54	1250	420	9.5	2.0	32.7	24	0.00017	-	-	-	
Oct-18	41	8.8	55	65.0	2.9	32	990	313	4.2	0.2	139	12	0.00022	-	-	-	
Nov-18	70	23.7	141	115	4.0	85	1180	522	7.3	0.3	302	33	0.00024	-	-	-	

bdl: below detection limit.

(-): not determined.

a: 2sd based on multiple analyses within analytical run.

b: 2sd used for plotting (the larger value of the analytical 2sd or 1.7‰/% Li in cut; see Table EA1b).

c: for samples marked by *, the column yield was between 99.0 and 99.8 % and a modified 2sd was used to account for uncertainty due to Li loss

Lithium isotope standards yield δ^7Li = +31.3 $\pm$ 0.6 (2sd, n=24) for seawater and δ^7Li = +2.5 ± 0.3 (n=5) for BCR-2.

Table EA3: Characterisation of local rocks and soils, including elemental composition data

Cave	Sample	δ^7Li	2sd	[Li]	Li/Na	Al/Ca	Al	Fe	Ti	Mg	Ca	Na	K	P	Mn	Ba	Sr	Rb	Li
		‰	‰	µg/g	mol/mol	mmol/mol	mg/g	mg/g	mg/g	mg/g	mg/g	mg/g	mg/g	µg/g	µg/g	µg/g	µg/g	µg/g	µg/g
Pippikin	Great Scar Limestone - bulk	-0.5	0.3	*0.27*	0.02	0.58	0.19	0.20	0.010	1.07	482	0.04	0.07	90	38	2.9	174	bdl	*0.27*
Pippikin	Great Scar Limestone - carbonate leach	0.0	0.7	*0.21*	0.02	0.24	0.07	0.06	bdl	1.06	435	0.04	bdl	120	43	2.9	170	bdl	*0.21*
Pippikin	Great Scar Limestone - residue	-10.3	0.3	*0.16*	0.02	0.78	0.13	0.17	0.006	0.69	249	0.02	0.02	bdl	22	1.4	104	bdl	*0.16*
Pippikin	interbedded shale, Arson Shaft, Ease Gill	-1.3	1.6	2260	3.40	141000	201	20.5	8.31	6.57	2.12	2.20	30.2	120	45	469	95.3	160	2260
Pippikin	Quaternary till, Ease Gill	-0.9	0.2	86	0.19	619000	57.7	28.4	3.49	3.05	0.14	1.53	11.3	230	352	139	49.2	70	86
Pippikin	peaty soil, overlying Pippikin cave	2.1	0.5	76	0.17	447000	61.7	17.3	3.65	2.93	0.21	1.47	9.70	100	28	117	53.5	62	76
Pippikin	cave sediment, floor of Pippikin cave	-0.8	0.2	100	0.14	5650	59.5	31.6	4.24	3.91	15.6	2.31	12.5	580	802	276	78.9	71	100
White Scar	Great Scar Limestone - bulk	-0.5	0.4	*0.89*	0.03	2.58	0.73	0.39	0.037	2.50	420	0.10	0.35	bdl	133	5.1	267	bdl	*0.89*
White Scar	Great Scar Limestone - carbonate leach	1.4	1.0	*0.12*	0.01	0.24	0.06	0.10	bdl	1.93	343	0.06	0.02	bdl	114	2.2	202	bdl	*0.12*
White Scar	Great Scar Limestone - residue	-0.3	0.4	*1.51*	0.10	10.5	1.32	0.58	0.097	1.62	187	0.05	0.44	bdl	76	5.8	129	bdl	*1.51*
White Scar	Yoredale Shale	-1.8	0.7	26	0.22	244	30.9	17.6	1.51	4.76	188	0.39	12.4	140	458	109	219	47	26
White Scar	Quaternary till	0.0	0.7	37	0.01	32400	50.4	31.5	3.28	5.01	2.31	13.0	11.0	550	879	378	88.0	60	37
BCR-2							71.3	93.2	13.2	19.5	47.7	23.0	14.9	1450	1410	683	325	41	8.7
Accuracy (%)							0%	-3%	-3%	-10%	-6%	-1%	1%	-8%	-7%	0%	-4%	-10%	-5%

bdl = below detection limit (at solution concentration analysed).
For the limestones (including leaches and residues), Li concentrations are based on the signal intensity from MC-ICP-MS (shown in italics).
For all other samples, Li concentrations are from ICP-OES.
All other elemental concentrations are from ICP-OES.
Accuracy for BCR-2 is assessed as the difference between measured and reference values (Jochum et al., 2016).

Reference:
Jochum K.P., Weis U., Schwager B., Stoll B., Wilson S.A., Haug G.H., Andreae M.O., Enzweiler J. (2016) Geostandards and Geoanalytical Research 40, 333-350.

Table EA4: Monthly precipitation and mean monthly temperature

Month	Precipitation[a] mm	Temperature[b] °C	Notes
Apr-16	*104*	*4*	c,d
May-16	*90*	*9*	c,d
Jun-16	*102*	*12*	c,d
Jul-16	*83*	*14*	c,d
Aug-16	*97*	*14*	c,d
Sep-16	95	12.22	
Oct-16	28	8.14	
Nov-16	157	2.76	
Dec-16	76	5.24	
Jan-17	81	2.86	
Feb-17	101	3.99	
Mar-17	140	5.23	
Apr-17	23	6.44	
May-17	54	10.53	
Jun-17	239	12.39	
Jul-17	183	12.97	
Aug-17	133	12.39	
Sep-17	182	10.65	
Oct-17	232	9.79	
Nov-17	140	5.04	
Dec-17	123	2.54	
Jan-18	96	2.83	
Feb-18	61	0.9	
Mar-18	78	2.36	
Apr-18	87	7.01	
May-18	21	12.02	
Jun-18	14	14.54	
Jul-18	68	15.93	
Aug-18	140	12.93	
Sep-18	114	10.23	
Oct-18	67	7.74	
Nov-18	69	5.62	
Dec-18	*177*	4.74	c

a: Monthly precipitation totals measured in Ingleton (except data in italics from Bingley).
b: Mean monthly temperatures measured outside the entrance to Pippikin cave (except data in italics from Bingley).
c: Monthly precipitation estimated from nearby weather station in Bingley (Bingley No 2, https://en.tutiempo.net/climate/united-kingdom.html), adjusted by a factor of 1.4 to account for the higher precipitation totals in the study area.
d: Mean monthly temperature estimated from nearby weather station in Bingley (Bingley No 2, https://en.tutiempo.net/climate/united-kingdom.html), adjusted by 1 °C to account for the lower temperatures in the study area.

Table EA5: Drip rates from stalagmate logger in Pippikin cave near to Pippikin C

Date	Daily mean drip rate drip/hour	Monthly smoothed drip rate drip/hour
24/08/16	125.0	
25/08/16	131.5	
26/08/16	125.7	
27/08/16	129.0	
28/08/16	129.9	
29/08/16	120.2	
30/08/16	124.3	
31/08/16	128.1	
01/09/16	126.5	
02/09/16	133.2	
03/09/16	140.4	
04/09/16	130.3	
05/09/16	125.7	
06/09/16	121.7	
07/09/16	132.1	129.6
08/09/16	137.9	129.7
09/09/16	137.4	130.1
10/09/16	131.2	130.3
11/09/16	132.0	130.3
12/09/16	136.6	130.3
13/09/16	131.3	130.7
14/09/16	129.7	131.2
15/09/16	131.9	131.7
16/09/16	127.2	132.1
17/09/16	122.2	131.8
18/09/16	128.3	131.1
19/09/16	124.7	130.8
20/09/16	129.8	130.7
21/09/16	134.9	130.9
22/09/16	129.8	130.7
23/09/16	127.4	130.1
24/09/16	142.8	129.6
25/09/16	133.3	129.4
26/09/16	128.1	129.2
27/09/16	129.1	128.9
28/09/16	132.7	129.1
29/09/16	140.4	129.5
30/09/16	141.1	129.7
01/10/16	139.6	129.9
02/10/16	124.2	130.2
03/10/16	118.8	130.1
04/10/16	120.7	130.0
05/10/16	123.1	129.8
06/10/16	127.8	129.6
07/10/16	128.1	129.7
08/10/16	119.9	129.9
09/10/16	121.0	129.5
10/10/16	126.0	129.1
11/10/16	126.5	128.9
12/10/16	126.6	128.6
13/10/16	136.9	128.0
14/10/16	141.2	127.3
15/10/16	138.1	126.7
16/10/16	134.8	126.2
17/10/16	128.9	126.2
18/10/16	127.8	126.5
19/10/16	121.1	127.1
20/10/16	123.5	127.8
21/10/16	128.5	128.0
22/10/16	131.9	128.1
23/10/16	135.1	128.3
24/10/16	129.6	129.0
25/10/16	122.2	129.4
26/10/16	120.7	129.5
27/10/16	121.0	129.3
28/10/16	114.3	129.0
29/10/16	118.7	128.0
30/10/16	123.9	127.5
31/10/16	125.8	127.2
01/11/16	124.5	127.6
02/11/16	127.4	128.5
03/11/16	137.9	129.2
04/11/16	143.0	129.6
05/11/16	133.9	129.9
06/11/16	130.8	130.2
07/11/16	126.3	129.8
08/11/16	142.5	129.1
09/11/16	138.0	128.8
10/11/16	128.9	128.9
11/11/16	121.2	129.0
12/11/16	127.2	129.1
13/11/16	112.9	128.9
14/11/16	121.4	128.7
15/11/16	125.9	128.5
16/11/16	142.5	128.5
17/11/16	155.1	128.3
18/11/16	140.5	127.8
19/11/16	135.6	127.2
20/11/16	139.4	126.9
21/11/16	139.1	126.6
22/11/16	122.9	126.6
23/11/16	109.0	125.9
24/11/16	113.8	125.5
25/11/16	122.5	125.4
26/11/16	125.6	125.4
27/11/16	115.9	125.4
28/11/16	114.4	125.9
29/11/16	117.0	126.1
30/11/16	120.0	126.2
01/12/16	123.3	125.3
02/12/16	122.9	123.7
03/12/16	122.6	123.0
04/12/16	124.6	122.7
05/12/16	124.2	122.6
06/12/16	123.9	122.3
07/12/16	126.5	122.3
08/12/16	120.4	123.1
09/12/16	126.0	123.5
10/12/16	125.7	123.6
11/12/16	120.4	123.1
12/12/16	127.4	122.7
13/12/16	129.0	122.8
14/12/16	127.0	122.9
15/12/16	128.3	123.0
16/12/16	114.7	123.2
17/12/16	107.5	123.3
18/12/16	118.9	123.1
19/12/16	127.9	123.3
20/12/16	137.8	123.1
21/12/16	130.1	122.8
22/12/16	121.3	122.6
23/12/16	132.2	122.5
24/12/16	125.5	122.4
25/12/16	128.4	123.0
26/12/16	109.1	123.6
27/12/16	105.0	123.8
28/12/16	115.9	124.2
29/12/16	121.6	124.1
30/12/16	121.3	123.8
31/12/16	130.6	123.9
01/01/17	125.5	124.2
02/01/17	117.5	123.9
03/01/17	128.0	123.4
04/01/17	119.5	122.7
05/01/17	114.3	122.4
06/01/17	121.6	122.6
07/01/17	117.9	122.4
08/01/17	122.1	122.4
09/01/17	144.6	122.3
10/01/17	137.0	122.9
11/01/17	133.8	124.0
12/01/17	142.5	124.8
13/01/17	122.2	125.2
14/01/17	118.3	125.6
15/01/17	120.3	125.6
16/01/17	114.4	125.9
17/01/17	111.7	126.7
18/01/17	112.8	127.4
19/01/17	115.9	128.1
20/01/17	121.0	128.7
21/01/17	128.0	128.6
22/01/17	126.9	128.8
23/01/17	124.3	128.8
24/01/17	125.8	127.6
25/01/17	127.7	126.9
26/01/17	136.6	126.4
27/01/17	139.6	125.7
28/01/17	136.1	125.6
29/01/17	132.2	125.7
30/01/17	131.0	125.8
31/01/17	133.6	126.0
01/02/17	141.5	126.2
02/02/17	149.3	126.4
03/02/17	140.0	126.7
04/02/17	132.4	126.9
05/02/17	120.1	126.9
06/02/17	123.2	127.1
07/02/17	121.1	127.6
08/02/17	108.4	127.9
09/02/17	117.4	127.5
10/02/17	119.0	127.4
11/02/17	120.0	127.3
12/02/17	120.1	127.6
13/02/17	122.1	127.6
14/02/17	121.3	127.5
15/02/17	120.0	126.9
16/02/17	119.4	126.8
17/02/17	119.0	126.4
18/02/17	125.5	126.0
19/02/17	124.4	125.4
20/02/17	128.3	125.2
21/02/17	135.1	125.1
22/02/17	136.6	124.7
23/02/17	136.9	125.0
24/02/17	113.7	125.3
25/02/17	133.5	125.4
26/02/17	137.3	125.0
27/02/17	145.8	124.8
28/02/17	132.1	124.6
01/03/17	126.4	124.9
02/03/17	117.6	125.4
03/03/17	137.2	125.8
04/03/17	139.2	126.2
05/03/17	128.0	126.5
06/03/17	112.0	126.6
07/03/17	115.2	126.5
08/03/17	120.2	125.6
09/03/17	108.1	124.5
10/03/17	119.3	123.9
11/03/17	127.1	124.2
12/03/17	120.7	124.0
13/03/17	109.4	123.7
14/03/17	112.8	123.2
15/03/17	114.8	123.1
16/03/17	130.3	123.4
17/03/17	137.5	123.6
18/03/17	129.2	122.8
19/03/17	131.5	122.2
20/03/17	134.6	121.6
21/03/17	126.9	121.7
22/03/17	125.5	121.8
23/03/17	107.2	122.0
24/03/17	106.2	122.6
25/03/17	116.9	122.8
26/03/17	123.2	122.5
27/03/17	127.1	122.5
28/03/17	130.4	123.2
29/03/17	128.2	123.7
30/03/17	131.1	124.2
31/03/17	134.7	123.9
01/04/17	125.0	123.4
02/04/17	111.6	122.9
03/04/17	121.2	122.1
04/04/17	111.0	121.4
05/04/17	113.6	121.0
06/04/17	119.6	120.8
07/04/17	124.3	121.3
08/04/17	127.5	121.9
09/04/17	125.8	122.5
10/04/17	115.8	122.6
11/04/17	123.4	122.4
12/04/17	130.5	122.2
13/04/17	127.0	122.0
14/04/17	130.3	121.9
15/04/17	121.6	121.9
16/04/17	121.6	121.7
17/04/17	114.3	121.5
18/04/17	108.2	121.0
19/04/17	112.2	121.0
20/04/17	115.1	121.1
21/04/17	121.0	121.0
22/04/17	119.6	120.6
23/04/17	126.3	119.9
24/04/17	134.4	119.7
25/04/17	126.0	120.3
26/04/17	120.2	120.7
27/04/17	124.7	120.6
28/04/17	123.3	120.2
29/04/17	128.3	119.3
30/04/17	134.5	119.0
01/05/17	118.2	118.6
02/05/17	105.0	118.6
03/05/17	107.8	119.0
04/05/17	109.4	119.1
05/05/17	116.3	119.0
06/05/17	118.9	118.6
07/05/17	110.2	118.5
08/05/17	106.7	117.8
09/05/17	121.6	116.7
10/05/17	133.4	116.0
11/05/17	133.9	115.7
12/05/17	127.2	115.4
13/05/17	114.9	114.8
14/05/17	103.2	114.3
15/05/17	113.0	113.4
16/05/17	109.2	113.0
17/05/17	116.5	113.1
18/05/17	117.7	113.2
19/05/17	117.3	113.4
20/05/17	112.1	113.3
21/05/17	108.0	113.7
22/05/17	117.3	114.2
23/05/17	104.1	114.3
24/05/17	101.3	114.3
25/05/17	105.9	113.4
26/05/17	110.6	112.8
27/05/17	116.1	112.5
28/05/17	104.8	112.3
29/05/17	114.2	112.4
30/05/17	108.5	112.4
31/05/17	103.7	112.6
01/06/17	109.4	112.1
02/06/17	110.8	111.5
03/06/17	113.7	111.1
04/06/17	113.7	111.0
05/06/17	132.0	111.0
06/06/17	126.2	110.9
07/06/17	109.0	111.3
08/06/17	120.1	111.8
09/06/17	108.9	112.1
10/06/17	114.0	112.3
11/06/17	118.6	112.1
12/06/17	108.1	112.8
13/06/17	106.9	113.2
14/06/17	113.7	113.8
15/06/17	114.2	114.0
16/06/17	100.8	113.9
17/06/17	101.5	113.6
18/06/17	106.2	113.5
19/06/17	108.0	113.4
20/06/17	107.1	112.6
21/06/17	115.9	112.2
22/06/17	114.5	112.2
23/06/17	115.6	111.8
24/06/17	116.6	112.1
25/06/17	114.8	112.2
26/06/17	112.5	112.0
27/06/17	123.8	111.8
28/06/17	127.9	111.9
29/06/17	126.7	111.6
30/06/17	108.2	111.5
01/07/17	105.9	111.5
02/07/17	104.5	111.6
03/07/17	108.5	111.9
04/07/17	110.9	112.4
05/07/17	109.0	112.7
06/07/17	113.6	112.9
07/07/17	109.1	113.0
08/07/17	108.4	112.9
09/07/17	116.3	112.6
10/07/17	116.8	112.6
11/07/17	115.1	113.1
12/07/17	101.3	113.1
13/07/17	108.4	113.0
14/07/17	106.5	112.8
15/07/17	110.2	113.4
16/07/17	101.9	113.8
17/07/17	104.7	114.2
18/07/17	113.7	114.8
19/07/17	123.5	115.3
20/07/17	117.3	115.5
21/07/17	121.5	115.4
22/07/17	116.9	115.6
23/07/17	112.3	115.9
24/07/17	107.9	116.0
25/07/17	114.7	115.7
26/07/17	128.0	115.6
27/07/17	124.2	116.4
28/07/17	124.6	116.6
29/07/17	121.3	116.8
30/07/17	123.9	117.3
31/07/17	118.3	117.8
01/08/17	117.2	118.4
02/08/17	126.7	118.8
03/08/17	126.4	118.8
04/08/17	114.0	118.7
05/08/17	110.9	118.2
06/08/17	114.8	118.1
07/08/17	118.2	118.2
08/08/17	118.8	118.7
09/08/17	109.3	118.7
10/08/17	111.1	118.3
11/08/17	124.1	118.0
12/08/17	116.3	117.6
13/08/17	112.8	117.4
14/08/17	123.3	117.3
15/08/17	118.2	117.3
16/08/17	121.3	117.2
17/08/17	126.3	116.5
18/08/17	124.1	116.2
19/08/17	113.2	116.7
20/08/17	108.0	117.0
21/08/17	112.9	117.2
22/08/17	116.6	117.1
23/08/17	121.1	117.4
24/08/17	116.3	118.2
25/08/17	114.8	118.8
26/08/17	114.1	119.2
27/08/17	112.7	119.6
28/08/17	117.2	120.0
29/08/17	118.8	120.0
30/08/17	119.5	119.8
31/08/17	113.0	119.6
01/09/17	108.3	119.3
02/09/17	115.9	119.0
03/09/17	128.0	119.0
04/09/17	121.9	119.1
05/09/17	120.2	119.4
06/09/17	114.4	119.5
07/09/17	128.6	119.2
08/09/17	134.4	119.2
09/09/17	126.8	119.2
10/09/17	138.2	119.1
11/09/17	127.0	119.1
12/09/17	124.8	119.3
13/09/17	124.4	119.3
14/09/17	112.8	119.4
15/09/17	114.4	119.7
16/09/17	118.1	120.4
17/09/17	113.3	120.5
18/09/17	112.1	119.8
19/09/17	113.9	119.9
20/09/17	121.5	119.7
21/09/17	117.1	119.7
22/09/17	114.7	119.6
23/09/17	114.9	119.0
24/09/17	116.1	118.9
25/09/17	111.4	118.6
26/09/17	112.2	118.7
27/09/17	121.9	118.5
28/09/17	118.7	118.3
29/09/17	122.0	118.4
30/09/17	121.7	118.8
01/10/17	130.9	119.2
02/10/17	118.5	119.4
03/10/17	108.6	119.9
04/10/17	124.1	120.7
05/10/17	113.9	120.9
06/10/17	114.2	121.5
07/10/17	126.2	121.4
08/10/17	116.8	121.0
09/10/17	123.7	120.7
10/10/17	128.6	120.2
11/10/17	131.2	119.6
12/10/17	116.0	118.5
13/10/17	119.9	118.1
14/10/17	116.2	117.2
15/10/17	124.9	116.2
16/10/17	131.3	115.2
17/10/17	118.4	115.0
18/10/17	127.0	115.0
19/10/17	137.3	114.4
20/10/17	128.2	114.3
21/10/17	135.6	113.7
22/10/17	111.6	112.6
23/10/17	103.5	111.9
24/10/17	107.0	110.8
25/10/17	97.2	109.6
26/10/17	93.5	108.5
27/10/17	88.9	107.9
28/10/17	105.5	106.9
29/10/17	94.6	105.9
30/10/17	91.4	104.9
31/10/17	103.8	103.5
01/11/17	112.4	102.6
02/11/17	106.6	101.4
03/11/17	107.9	99.9
04/11/17	110.7	98.6
05/11/17	94.8	97.4
06/11/17	93.3	97.1
07/11/17	96.6	97.6
08/11/17	89.8	97.2
09/11/17	93.8	96.9
10/11/17	96.6	96.7
11/11/17	98.3	96.6
12/11/17	89.8	96.4
13/11/17	86.1	96.3
14/11/17	94.5	96.3
15/11/17	91.5	96.0
16/11/17	91.1	95.8
17/11/17	88.8	96.1
18/11/17	92.9	96.2
19/11/17	89.9	96.2
20/11/17	100.6	96.9
21/11/17	102.3	98.2
22/11/17	117.1	99.4
23/11/17	96.9	100.2
24/11/17	86.1	101.3
25/11/17	87.6	102.8
26/11/17	86.0	103.5
27/11/17	99.7	104.3
28/11/17	92.9	105.8
29/11/17	90.4	107.0
30/11/17	95.4	107.4
01/12/17	107.2	107.8
02/12/17	114.4	108.5
03/12/17	112.0	108.8
04/12/17	109.4	109.4
05/12/17	115.9	109.6
06/12/17	132.9	109.8
07/12/17	132.0	109.5
08/12/17	114.5	110.1
09/12/17	125.7	111.6
10/12/17	142.3	113.3
11/12/17	118.8	114.7
12/12/17	115.2	115.4
13/12/17	131.5	116.2
14/12/17	128.6	117.4
15/12/17	104.9	118.1
16/12/17	102.6	118.5
17/12/17	110.0	118.3
18/12/17	101.6	118.5
19/12/17	106.3	118.5
20/12/17	107.3	118.6
21/12/17	109.6	117.8
22/12/17	106.4	116.5
23/12/17	115.9	116.0
24/12/17	129.9	115.8
25/12/17	139.2	115.4
26/12/17	129.9	115.3
27/12/17	120.0	114.9
28/12/17	115.7	114.1
29/12/17	127.7	113.7
30/12/17	114.8	114.3
31/12/17	119.4	115.3
01/01/18	108.9	115.8
02/01/18	116.7	116.2
03/01/18	111.5	116.4
04/01/18	117.2	116.5
05/01/18	110.1	116.5
06/01/18	94.2	116.7
07/01/18	99.3	116.4
08/01/18	118.7	115.8
09/01/18	130.2	115.2
10/01/18	116.4	114.6

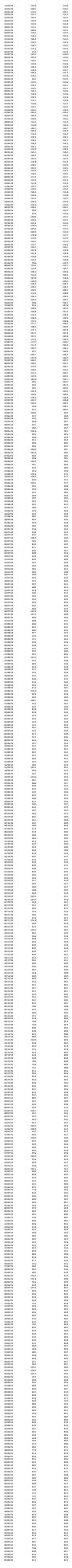

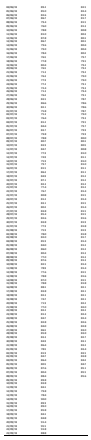

Figure EA1: Cave survey of Pippikin cave, showing drip-water sampling locations Pippikin A and D

Reproduced with permission from: Red Rose Cave and Pothole Club (2016) Survey of Mistral Entrance into Pippikin area of the Easegill Cave System

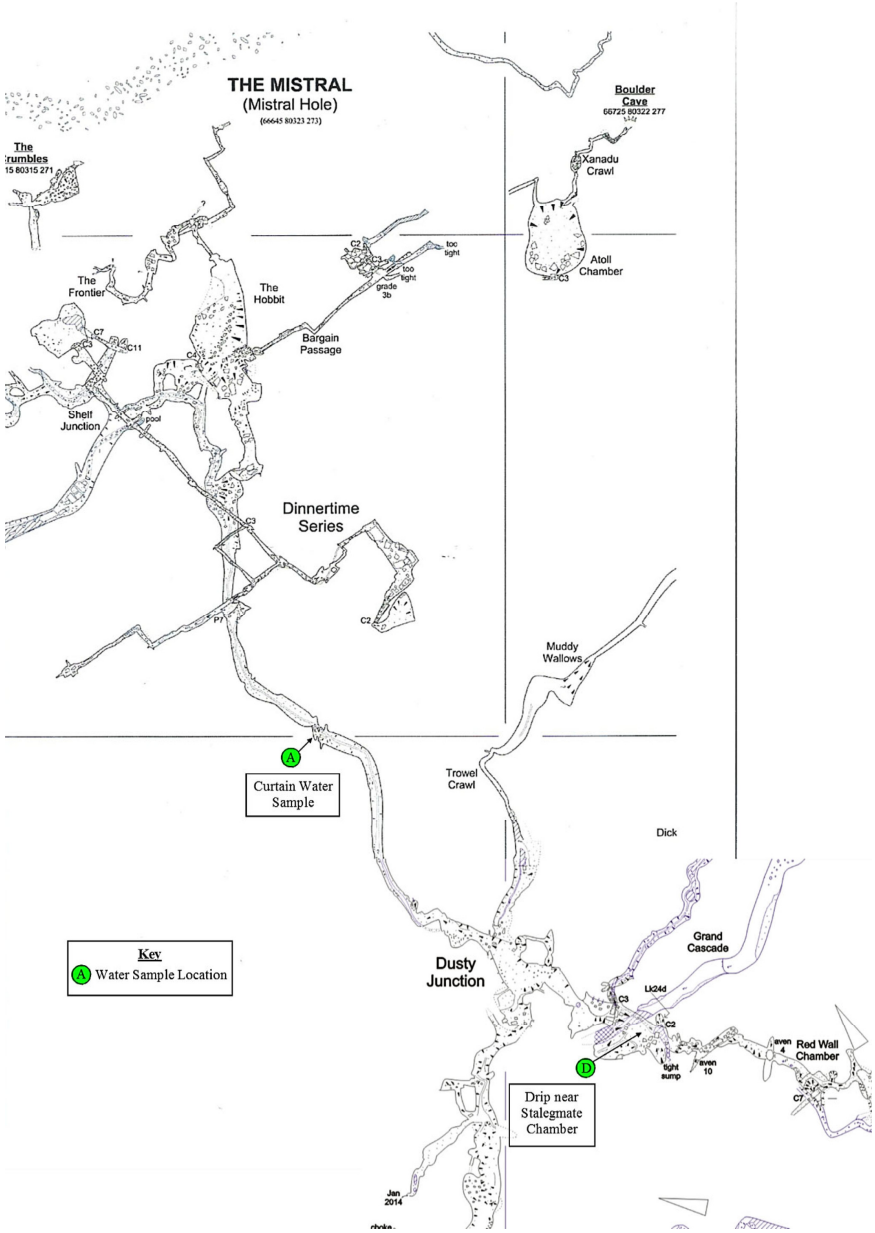

Figure EA2: Cave survey of White Scar Cave, showing drip-water sampling locations White Scar 1 and 3
Reproduced from: Waltham A.C. (1977) White Scar Cave. *Transactions of the British Cave Research Association* **4** (3), 345-353.